Molecular basis for potent B cell responses to antigen displayed on particles of viral size

Jeremy F. Brooks[1†], Julianne Riggs[1,2†], James L. Mueller[1], Raisa Mathenge[1], Wei-Yun Wholey[3], Sekou-Tidiane Yoda[3], Vivasvan S. Vykunta[1,4], Wei Cheng[3,5]*, Julie Zikherman[1]*

[1] Division of Rheumatology, Rosalind Russell and Ephraim P. Engleman Arthritis Research Center, Department of Medicine, University of California, San Francisco, California 94143 USA

[2] Biomedical Sciences Graduate Program, University of California, San Francisco, California 94143 USA

[3] Department of Pharmaceutical Sciences, 428 Church Street, University of Michigan, Ann Arbor, Michigan 48109, USA

[4] Department of Molecular and Cell Biology, University of California Berkeley, California 94720, USA

[5] Department of Biological Chemistry, 1150 W. Medical Center Dr., University of Michigan Medical School, Ann Arbor, Michigan 48109, USA

†: Both authors contributed equally to this work.

*Corresponding authors:

Dr Julie Zikherman
513 Parnassus Avenue
Room HSW1201E, Box 0795
San Francisco, CA, 94143-0795
Tel: (415)-476-1689
email address: Julie.zikherman@ucsf.edu

Dr Wei Cheng
University of Michigan
428 Church Street
Ann Arbor, MI, 48109-1065
Tel: (734) 763-3709
Fax: (734) 615-6162

email address: chengwe@umich.edu

Keywords: B cell receptor (BCR) signaling, virus-like structures, epitope density, B cell tolerance, inhibitory co-receptors, Lyn Src Family Kinas (SFK), immunoreceptor tyrosine-based inhibitory motif (ITIM)

Abstract

Although it has long been appreciated that multivalent antigens – and particularly viral epitope display – produce extremely rapid, robust, and T-independent humoral immune responses, the biochemical basis for such potency has been incompletely understood. Here we take advantage of a set of neutral liposomes of viral size that are engineered to display affinity mutants of the model antigen (Ag) hen egg lysozyme at precisely varied density. We show that particulate Ag display by liposomes induces highly potent B cell responses that are dose- and density-dependent but affinity-independent. Titrating dose of particulate, but not soluble, Ag reveals bimodal Erk phosphorylation and cytosolic calcium increases. Particulate Ag induces signal amplification downstream of the B cell receptor (BCR) by selectively evading LYN-dependent inhibitory pathways, but *in vitro* potency is independent of CD19. Importantly, Ag display on viral-sized particles signals independently of MYD88 and IRAK1/4, but activates NF-κB robustly in a manner that mimics T cell help. Together, such biased signaling by particulate Ag promotes MYC expression and reduces the threshold required for B cell proliferation relative to soluble Ag. These findings uncover a molecular basis for highly sensitive B cell response to viral Ag display and remarkable potency of virus-like particle vaccines that is not merely accounted for by avidity and BCR cross-linking, and is independent of the contribution of B cell nucleic acid-sensing machinery.

Introduction

Multivalent antigens, including viral structures, produce robust B cell responses that can engage – but do not require – T cell help, and design of virus-like particle (VLP) vaccines is predicated in part upon this observation[1,2]. Particulate HIV immunogens with high valency can recruit precursor B cells expressing rare and low-affinity germline-encoded B cell receptors (BCRs) into both the extra-follicular and germinal center responses[3-5]. Indeed, highly organized epitope display on the surface of viral particles has long been proposed to function as an immunogenic signal of 'foreignness,' and can trigger robust T-independent antibody responses that may not require TLR engagement[1,2,6-11].

Although the structural basis for BCR triggering by various forms of antigen (Ag) continues to be debated[12], potent cellular responses to multivalent epitopes are assumed to reflect cross-linking of Ag-receptors. Dintzis et al. reported that a minimum number of haptens (>12) spaced appropriately along a linear backbone (≅ 10 nm) was essential to trigger a T-independent humoral immune response *in vivo* and proposed the "immunon" model, postulating a requirement for clustering of a minimum number of hapten-binding receptors[8]. More recently, "molecular origami" has defined an optimal spacing and valency of high affinity epitopes to trigger BCR-induced calcium entry[13]. However, the mechanistic basis for potent (and T-independent) B cell responses to density of epitopes displayed on particles of viral size is not fully understood. Specifically, whether such potency is purely a function of avidity and receptor cross-linking, or also reflects a qualitatively unique mode of B cell triggering by this biologically significant class of Ag is unknown.

By contrast, the molecular basis for B cell responses to membrane-associated Ag presented on the surface of cells has been extensively explored[14-18]. Tethering of non-stimulatory monovalent haptens to a membrane is sufficient to trigger BCR signaling[19]. Membrane-associated Ag also dramatically reduces the threshold for B cell activation relative to soluble Ag, and impacts affinity discrimination[20-24]. Membrane Ags have been postulated to achieve such potency by reorganizing membrane structure upon contact with B cells to generate initially BCR microclusters, and subsequently an immune-synapse-like (IS) contact interface via actin remodeling[14,15,20,23]. This is associated with recruitment of CD19 co-receptor into the IS and exclusion of inhibitory co-receptors such as CD22 and FcγRIIb along with associated phosphatase (PTPase) SHP1[20,25,26]. Membrane-associated Ags require CD19 for downstream signaling *in vitro* (as does B cell signaling triggered by actin

depolymerization), while soluble Ag does not[23,27-29]. Whether exclusion from the IS of inhibitory machinery is also essential for potent responses to membrane Ag is less clear [20,25,26,30].

However, Ag captured and presented on the membrane of macrophages and dendritic cells, and particles of viral size differ from one another not only in size of interface presented to responding B cells but also in fundamental biophysical properties such as actin dynamics, pulling force, and BCR internalization. B cells encounter and respond to membrane-associated Ag in a variety of physiologic contexts, such as when Ag is captured and presented on the surface of follicular dendritic cells during affinity maturation. Direct encounter between B cells and viruses – as well as multivalent VLP vaccines – occurs *in vivo* at early time points and the nature of this interaction can define the trajectory of the subsequent immune response[1,31-37].

To understand how B cells signal in response to Ag display on viruses, here we take advantage of a novel set of viral-sized liposomes that are engineered to display affinity mutants of the model Ag hen egg lysozyme (HEL) but lacking nucleic acid cargo[38]. These liposomes display a programmable range of HEL epitope density on their surface that mimics the spectrum observed on naturally occurring viruses[39]. We show that Ag display on these synthetic particles of viral size induces potent and remarkably prolonged B cell responses that are density-dependent but affinity-independent, and do not rely on MYD88/IRAK1/4 signaling. These responses are characterized by bimodal Erk phosphorylation and cytosolic calcium entry at the single cell level suggesting digital behavior, and are sufficient to activate anergic B cells. Signaling in response to these particles requires SYK, BTK, and PI3K enzyme activity, implicating the canonical BCR signaling pathway. We show that such particulate Ags trigger robust signal amplification downstream of the BCR by evading LYN-dependent inhibitory pathways, but *in vitro* potency is independent of CD19 – in contrast to membrane Ag presented on APCs. Particulate Ag also trigger uniquely robust NF-κB activation, MYC expression, cell growth, survival, and reduce the threshold for B cell proliferation in a manner that mimics T cell help. This reveals a new mechanism by which B cells recognize virus-like Ag display as stand-alone danger signal – independent of nucleic acid cargo – that does not rely exclusively on avidity and BCR cross-linking. This in turn helps explain how extremely rapid, protective, and T-independent B cell responses to low doses of virus or VLP are mounted.

66 Results

67 **Antigen display on particles of viral size induce potent B cell responses that are density-**
68 **dependent but affinity-independent**

69 We constructed a library of neutral, unilamellar liposomes of viral size (approx. 120nm
70 diameter) conjugated via maleimide chemistry to a very well-characterized model Ag (hen egg
71 lysozyme; HEL), as previously described by us (**Figures 1A, Supplementary Figures 1A,**
72 **B)**[38]. These liposomes display HEL protein in a specific orientation and at a programmable
73 density in order to mimic the range of epitope display on bona fide viruses[39]. Importantly, to
74 isolate the impact of virus-like Ag display on B cell responses, the synthetic virus-like
75 structures (SVLS) generated for this study harbor phosphate-buffered saline on the interior and
76 lack any packaged nucleic acid content such that conjugated surface proteins are the only
77 immunogenic component.

78 We further took advantage of previously characterized amino acid substitutions in the
79 HEL protein that reduce its affinity for the Hy10 BCR relative to native ("WT") HEL [40]. HELD
80 refers to a HEL mutant carrying double mutations R73E, D101R (K_a to the Hy10 BCR =
81 8.0×10^7 M^{-1}) and HELT refers to a HEL mutant carrying triple mutations R21Q, R73E, D101R
82 (K_a = 1.5×10^6 M^{-1}) **(Supplementary Figures 1A)**[40]. Importantly, the micromolar affinity of
83 the mutant HELT protein for the Hy10 BCR is comparable to typical germline-encoded naïve
84 B cell affinities for polyclonal Ags[3]. This feature enables us to probe physiologically relevant
85 interactions and to extrapolate our findings to a naturally occurring naïve B cell repertoire. We
86 confirmed that the soluble HEL mutant proteins we generated triggered responses in an
87 affinity- and concentration-dependent manner in naïve B cells from so-called "MD4" mice that
88 express the Hy10 IgM/IgD BCR transgene and co-express a reporter of BCR signaling,
89 NUR77/*Nr4a1*-eGFP BAC Tg[41,42] **(Figure 1B),** consistent with previous reports[38,40,43].

90 By combining engineered liposomes with recombinant HEL proteins, we can vary both
91 density and affinity of conjugated surface epitopes (**Figures 1A, Supplementary Figures 1A,**
92 **B).** We decorated liposomes with either the moderate affinity mutant (HELD) or the low
93 affinity mutant (HELT) at matched densities, between 3-500 epitopes per liposomal particle
94 (approximately 60 to 10,000 molecules per μm^2); these HEL-engineered SVLS are referred to
95 herein as particulate HEL or pHEL – by contrast to soluble HEL or sHEL **(Figure 1A,**
96 **Supplementary Figure 1B)**.

97 The concentration of HELD and HELT proteins required to upregulate NUR77-GFP in
98 MD4 reporter B cells expressing the Hy10 BCR was dramatically reduced (by over 3 orders of
99 magnitude) when tethered to SVLS at a density of approximately 250-290 epitopes per
100 liposome **(Figure 1C, D)**, termed epitope density or ED herein. For example, the EC_{50} value
101 for sHELT in this assay was on the order of 500 ng/ml, consistent with prior reports[38,40,43], but
102 nearly 5000-fold lower concentrations of HELT protein when tethered to SVLS (pHELT) could
103 elicit detectable eGFP upregulation in Ag-specific reporter B cells after 24 hours of *in vitro*
104 culture. Interestingly, a comparable 1000-fold boost in potency was previously described for
105 intermediate affinity HEL (K_a similar to HELD mutant in our study) tethered to a cell
106 membrane[20]. Non-transgenic (wild-type) NUR77-GFP reporter B cells admixed with MD4
107 reporter B cells in culture failed to upregulate GFP in response to pHEL confirming that Ag-
108 specific BCR was required for the response **(Supplementary Figure 1C)**. Similarly, the
109 response was not simply due to the physical properties of the particles themselves, because
110 "naked" liposomes (pLIP02) without conjugated HEL protein also failed to induce NUR77-
111 GFP in MD4 B cells **(Supplementary Figure 1C)**. Impressively, a single batch of pHEL SVLS
112 stored at 4 degrees was stable for more than 400 days following its synthesis without loss of
113 potency **(Supplementary Figure 1D)**.

114 To study effects of ED among engineered liposomes, pHEL library constructs were
115 compared according to liposome concentration across a broad titration in order to control for
116 liposome number. B cells are highly sensitive to ED of pHELD and upregulated NUR77-
117 GFP in a density-dependent manner **(Figure 1E)**. Interestingly, B cell activation did not scale
118 continuously with ED for low affinity pHELT **(Supplementary Figure 1E)**, indicating that
119 there may be an optimum ED for display that is not simply the highest. Moreover, even
120 particles with as few as 3 conjugated HELT molecules could trigger NUR77-GFP
121 upregulation at particle concentration < 1pM **(Supplementary Figure 1F)**, suggesting that
122 tethering of Ag to SVLS even in the absence of extensive BCR cross-linking confers many
123 orders of magnitude higher potency than soluble Ag (**Figure 1B)**. Similar results were
124 obtained with an orthogonal readout of B cell activation, surface CD69 upregulation, and also
125 segregated by high and low ED **(Supplementary Figure 1G)**. B cell sensitivity to ED was
126 also observed *in vivo* (doi: https://doi.org/10.1101/2023.02.20.529089).

127 Prior work has demonstrated that conjugating similar HEL Ags to large cell surface
128 membranes can override affinity discrimination[21,22], although B cells still exhibit affinity-
129 sensing behavior in response to Ag presented on cells[23,24]. Here we show that conjugating

130 HEL affinity mutants to SVLS also bridges affinity gaps; SVLS bearing either HELD or
131 HELT Ag at matched ED were capable of inducing equivalent levels of NUR77-GFP
132 expression despite a reproducible gap in affinity and potency measured for these proteins in
133 soluble form **(Figure 1B, F, Supplementary Figure 1F)**, indicating that B cells could be
134 activated even by low affinity Ag displayed on small particles of viral size.

135 Collectively our data demonstrate that Ag display on SVLS are highly potent for
136 inducing B cell responses in a density-dependent but affinity-independent manner. Importantly,
137 these 24 hr assays enabled us to select "equipotent" doses of pHEL and sHEL for further study
138 of both upstream and downstream B cell responses. Specifically, 1pM pHELD/pHELT
139 liposomes conjugated with high ED (250-290 epitopes / SVLS) corresponds to 250-290pM (≅
140 4ng/ml) of HEL protein. Similarly, 1pM of lower ED pHEL liposomes (61-64 epitopes / SVLS)
141 corresponds to 61-64pM (≅ 1ng/ml) HEL protein (**Supplementary Figure 1B**). Throughout
142 this manuscript, 1pM pHEL doses were compared to much higher, maximally potent sHEL
143 concentrations of 1μg/ml (≅ 64nM HEL protein) except where dose is explicitly titrated (0.1-
144 10pM range). Indeed, high doses of soluble stimuli – especially low affinity mutants of HEL –
145 are necessary to trigger detectable B cell signaling and activation. These 'equipotent' doses
146 used for subsequent assays therefore corresponded to 250-1000x differences in HEL
147 concentration between pHEL and sHEL comparators depending on ED (**Figures 1C, D**).

148

149 **Low doses of pHEL drive robust B cell proliferation in an affinity-independent manner**

150 We next sought to compare the effect of soluble and particulate Ag display on B cell
151 proliferation *in vitro*. Despite absence of co-stimulation, B cells proliferated robustly to both
152 sHEL and pHEL equipotent stimuli when co-cultured with BAFF as assessed by vital dye
153 dilution **(Figure 1G, H)**. As evident with 24 hr NUR77-eGFP upregulation (**Figure 1A**),
154 proliferation in response to sHEL was highly dependent upon both dose and affinity of Ag and
155 exhibited EC_{50} in the same order of magnitude for both assays (**Figure 1G**). By contrast, very
156 low doses of pHELD/T (1pM ≅ 1-4ng/ml HEL concentration) were sufficient to drive robust
157 proliferation. This proceeded in a concentration- and density-dependent, but affinity-
158 independent, manner (**Figure 1H**). Interestingly, we found that reducing the concentration of
159 high ED SVLS allowed us to visualize a small fraction of B cells that had undergone many
160 rounds of division **(Figure 1H, arrowheads)**. This outcome was not evident when ED was
161 reduced nor when B cells were stimulated with sHEL **(Figure 1G, H).** These data suggest that

162 even a small number of pHEL particles might be sufficient for maximal B cell activation;
163 reducing pHEL concentration lowers the number of cells engaged, but not extent of activation
164 on a single cell level, conferring an all-or-none response. Importantly, potent B cell
165 proliferation in response to pHEL are not attributable to engagement of marginal zone (MZ) B
166 cells – which exhibit unique biology and play a critical role in early *in vivo* responses to T-
167 independent multivalent Ags – because these assays are performed with lymph node rather than
168 spleen as a source of exclusively follicular B cells[44].

169

170 **pHEL triggers highly robust BCR signaling that is insensitive to epitope affinity**

171 We next took advantage of these unique tools to explore the biochemical basis for such
172 robust B cell responses to Ag displayed on virus-sized particles. We first sought to dissect early
173 signaling events downstream of BCR engagement by soluble and particulate Ag. As described
174 above, we selected 'equipotent' concentrations of soluble and particulate stimuli (1pM pHEL
175 and 1µg/ml sHEL) that induced comparable levels of downstream NUR77-GFP **(Figure 1)** in
176 order to determine how signaling at early time points after BCR engagement differed between
177 these modes of Ag display. We compared these stimuli to maximally potent anti-IgM Fab'2
178 (10µg/ml) as a reference because antibody-mediated BCR cross-linking is very well-
179 characterized.

180 At early time points after stimulation (3 min), pHELD and sHELD induced comparable
181 phospho-Erk (pErk), but signaling induced by pHELD was much more robust, peaking at 20
182 minutes (**Figure 2A**). Importantly, this time course was comparable whether pHEL and sHEL
183 stimuli were pre-bound to MD4 B cells at 4C prior to 37C stimulation, or acutely admixed at
184 37C, implying that delayed peak was not attributable to binding kinetics of pHEL (DNS). As
185 seen for NUR77-eGFP upregulation, naked liposomes without conjugated HEL protein failed
186 to induce any detectable pErk. Similar to pHELD, pHELT was also highly potent for pErk
187 induction with similar kinetics (**Figure 2A, B**). Unlike sHELD, sHELT was largely unable to
188 trigger detectable pErk at any time point assayed (**Figure 2B, C**). Importantly, pErk levels
189 were comparable when B cells were stimulated with either pHELT or pHELD of matched high
190 ED (**Figure 2C**), suggesting that even early BCR signaling events do not discriminate affinity
191 when Ag is presented on particles of viral size, and this was true across extensive titration of
192 pHEL concentration **(Figure 2D).** S6 phosphorylation requires a lower BCR signaling
193 threshold than Erk phosphorylation and continues to increase over the time course studied (2

194 hrs). Very low doses of pHELT triggered S6 phosphorylation more robustly than 1μg/ml
195 sHELT (**Supplementary Figure 2A, B**). Importantly, as seen for pErk, both pHELT and
196 pHELD induced comparable pS6 levels and exhibited no evidence of affinity discrimination
197 (**Supplementary Figure 2C**).

198 We next measured cytosolic calcium changes following pHELD stimulation by loading
199 MD4 B cells with the calcium indicator Indo-1 and analyzing acutely activated cells by flow
200 cytometry. Although the response to pHELD was slower to reach peak intra-cellular calcium
201 concentrations than with soluble stimuli (by almost 60 seconds), responding cells ultimately
202 achieved a much higher peak that was comparable to ionomycin stimulation, suggesting it was
203 maximal within the dynamic range of this assay **(Figure 2E, F)**. In contrast to maximal doses
204 of either anti-IgM or sHELD which induced rapid but very short-lived intra-cellular calcium
205 increases with uniform kinetics across the entire B cell population, doses as low as 1pM
206 pHELD exhibited delayed but remarkably prolonged calcium increases among a subset of cells
207 (**Figure 2E, F**). To our surprise, the response exceeded 10 minutes; B cells with intra-cellular
208 calcium levels that were clearly above background were detectable at the latest time point
209 assayed with only a very slow decay back to baseline. By contrast, duration of peak intra-
210 cellular calcium triggered by soluble stimuli was on the order of 60 seconds (**Figure 2E, F**).
211 Importantly, we do not interpret this to merely represent delayed and inhomogeneous B cell
212 activation in response to SVLS, because nearly all B cells at the population level exhibited
213 maximal intra-cellular calcium levels by 90 seconds following 1pM pHELD stimulation, while
214 high intracellular calcium was still seen in a subset of cells more than 500 seconds later (**Figure
215 2F**). We cannot exclude the possibility that capture of additional pHEL by unoccupied BCRs
216 does prolong calcium signaling. However, we present data later in this study to suggest that
217 rapid signal termination in response to soluble Ag requires active engagement of inhibitory
218 pathways that are evaded by particulate Ag.

219 Robust signaling triggered by pHEL was not due to selective responses by MZ B cells
220 because lymph node samples lacking MZ B cells exhibited comparable pErk response as
221 splenic B cells **(Supplementary Figure 2D).** Similarly, gating on follicular and MZ B cells
222 independently on the basis of surface CD21 and CD23 expression **(Supplementary Figure
223 2E-I)** revealed robust signaling in both B cell subsets. Indeed, follicular B cells were
224 reproducibly more responsive to pHEL than either immature or MZ B cells – regardless of
225 readout. By contrast, sHEL and anti-IgM stimuli signaled most robustly in MZ B cells.

226

227 **pHEL trigger bimodal signaling that is sensitive to dose and epitope density but not**
228 **affinity**

229 Strikingly, single cell resolution of pErk responses afforded by phosflow revealed that
230 the fraction of responding cells was reduced with lower doses of pHEL, but even very low
231 concentrations of pHELT or pHELD could induce comparable and maximal levels of pErk in
232 a small fraction of B cells in culture (**Figure 3A**). This bimodal signaling was reminiscent of
233 the proliferative response of B cells to pHELT/D with high ED (**Figure 1H**). Reducing ED
234 also reduced pErk MFI but in a bimodal manner, suggesting "all-or-none" digital responses to
235 pHEL by single B cells (**Figure 3B**). This observation extended as well to pHEL with ultralow
236 ED (pHELT ED 3). Strikingly, such ultralow ED particles were nevertheless many orders of
237 magnitude more potent than soluble Ag, inducing robust pErk response at 10pM SVLS
238 (equivalent to 30pM ≅ 0.4ng HELT protein) (**Supplementary Figure 2J**). This corresponded
239 well to robust Nur77-eGFP induction by these reagents (**Supplementary Figure 1F**) and
240 reinforced the possibility that pHEL potency was not merely attributable to extensive BCR
241 cross-linking by individual SVLS particles.

242 To our surprise even at the earliest time points we could assess, all pHEL calcium
243 responses were bimodal, in marked contrast to soluble stimuli (**Figure 3C-E**); as with pErk,
244 reducing concentration of pHEL decreased fraction of responding cells but not intra-cellular
245 calcium level among responding cells (**Figure 3A, D**). These bimodal calcium responses were
246 sensitive to dose and ED, and strikingly appeared to give a reduced maximal Indo-1 (ca2+
247 bound/unbound) ratio with low ED. Importantly, these responses to SVLS were insensitive to
248 affinity in marked contrast to soluble stimuli. Such bimodal single cell behavior in response to
249 pHEL suggests that particulate Ag triggers signal amplification that may operate at a node
250 upstream of both MAPK and calcium pathways.

251 We next took advantage of a well-studied model of B cell tolerance; Hy10 BCR Tg B
252 cells that develop and mature in hosts expressing sHEL as a self-antigen (MD4.ML5 Double
253 Tg mice) exhibit canonical features of anergy, including IgM downregulation and suppressed
254 proximal BCR signal transduction[42,45]. We found that both soluble stimuli and pHEL triggered
255 dampened responses in self-reactive, anergic MD4.ML5 B cells relative to naïve MD4 B cells
256 (**Figure 3F**). However, calcium increases triggered by 1pM pHEL in anergic B cells was
257 nevertheless more robust and considerably more prolonged than maximal soluble stimulation

258 of naïve MD4 B cells (**Figure 3F**). Perhaps most strikingly, pHEL triggered bimodal behavior;
259 a fraction of anergic MD4.ML5 cells exhibited maximal calcium entry that was comparably
260 robust and prolonged relative to responding non-anergic, naive MD4 B cells (**Figure 3G**). This
261 suggested that a fraction of even deeply anergic B cells could be "re-awakened" by virus-like
262 Ag display. Indeed, ncreased amplitude and duration of cytosolic calcium increases can in turn
263 activate transcriptional pathways such as NF-κB that are normally suppressed by anergy[46,47].

264

265 **pHEL requires canonical BCR signaling pathway but is independent of MYD88 and**
266 **IRAK1/4**

267 Because pHEL trigger remarkably robust signal transduction in B cells, we sought to
268 exclude a role for any contaminating nucleic acids that could be delivered via pHEL to
269 endosomal TLRs. To do so, we first took advantage of a highly selective IRAK1/4 inhibitor
270 (R568, Rigel Pharmaceuticals). This drug blocked CpG-induced pErk and pS6 but did not
271 inhibit pHEL signaling **(Figures 4A, B)**. Similarly, deletion of MYD88 completely suppressed
272 signaling by LPS and CpG but had no impact on other pathways (such as BCR or CD40) as
273 expected (**Figure 4C, D**). Importantly, MYD88 was completely dispensable for pHEL
274 responses *in vitro* (**Figures 4C, D**). Conversely, pHEL responses were fully dependent upon
275 activity of canonical BCR pathway signaling molecules like SYK, BTK and PI3K[48]; small
276 molecule inhibitors of these enzymes completely eliminated downstream induction of pErk in
277 response to pHEL, but did not impair CpG-induced Erk phosphorylation via endosomal TLR9
278 (**Figure 4E-H)**.

279

280 **pHEL trigger robust signal amplification downstream of the BCR**

281 Robust bimodal or digital signaling responses suggest that pHEL may trigger signal
282 amplification downstream of the BCR relative to soluble Ag. To investigate this mechanism,
283 we comprehensively analysed the most proximal biochemical events triggered in B cells at
284 early time points after stimulation with anti-IgM, sHELD and pHELD. We selected a 3-minute
285 stimulation for Western blot analysis, because pHELD and sHELD induce comparable Erk
286 phosphorylation at this time point as detected by intracellular staining (**Figure 2A**). Although
287 downstream readouts like pErk and pIKK were robustly induced by both sHEL and pHEL after
288 3 minutes, to our surprise total tyrosine phosphorylation (probed with 4G10 mAb) was virtually

289 undetectable following pHEL stimulation (**Figure 5A, B**). Similarly, tyrosine phosphorylation
290 of the BCR itself (CD79A), SYK, and PI3K were also robustly induced by soluble stimuli, but
291 virtually undetectable by western blot for pHEL stimulation **(Figure 5C, D)**. Phosphorylation
292 of PLCγ2 at Y1217 is a key proximal event triggered by BCR engagement that occurs upstream
293 of BTK[49]. This was also induced by soluble stimuli, but not increased with pHEL.
294 Nevertheless, although phosphorylation of proximal signaling nodes in response to pHEL was
295 below the limits of detection by western blotting, pHEL responses do engage and require
296 enzymatic activity of canonical BCR signaling molecules SYK, BTK, and PI3K because small
297 molecule inhibitors of these enzymes completely prevented downstream induction of pErk in
298 response to pHEL as noted earlier **(Figure 4E-H)**[48].

299 Consistent with calcium kinetics (**Figures 2E, F, 3D**), robust pErk and pIKK induction
300 by pHEL indicated that BCR engagement occurred by 3 minutes (**Figure 5B**) and that
301 undetectable phosphorylation of the proximal BCR signaling cascade was not attributable to
302 selection of an early time point. This discordance between proximal and distal signaling led us
303 to hypothesize that a small number of BCRs engaged by low concentration pHEL induced
304 proximal tyrosine phosphorylation below the limits of detection, and subsequent downstream
305 signal amplification resulted in robust downstream phosphorylation of Erk and IKK.
306 Conversely, these data suggest that potent downstream signaling by pHEL was not merely a
307 consequence of enhanced proximal BCR engagement (i.e. extensive BCR cross-linking) as
308 such a mechanism would be anticipated to produce robust phosphorylation at the most proximal
309 signaling nodes such as pCD79A and pSYK. This argues against mere avidity alone as a
310 mechanism for pHEL potency.

311 The second messenger PIP3 represents a key signaling intermediate that dynamically
312 accumulates at the plasma membrane to nucleate the assembly of the BCR 'signalosome' and
313 serves as a node for tuning BCR signal amplification[50]. AKT T308 phosphorylation is mediated
314 by PDK1 and is highly dependent upon PIP3 for recruitment of both AKT and PDK1 via their
315 PH-binding domains[51,52]. By contrast to proximal tyrosine phosphorylation, detectable AKT
316 serine/threonine phosphorylation was induced by both sHEL and pHEL at 3 minutes (**Figures**
317 **5C-E**). BTK autophosphorylation at Y223 also depends upon recruitment to PIP3 and
318 dimerization[53,54], and is measurably induced by pHEL (**Figure 5C, E**). Detectable
319 phosphorylation of these sites following pHEL stimulation suggested that local PIP3
320 generation by PI3K at the membrane might serve to disproportionately amplify signaling in
321 response to pHEL. Importantly, although PI3K phosphorylation is undetectable after pHEL

322 stimulation (**Figures 5C, D**), downstream pHEL signaling is nevertheless sensitive to PI3K
323 inhibition (**Figure 4G, H**).

324

325 **Potent signaling by pHEL *in vitro* is not dependent upon CD19**

326 PIP3 abundance at the membrane in response to BCR stimulation is regulated both at
327 the level of its generation and its degradation[48,50]. The CD19 coreceptor plays an important role
328 in amplifying PIP3 production by PI3K in response to BCR stimulation. Moreover, CD19 is
329 co-clustered with BCR upon encounter with cell–membrane associated Ags or via
330 complement-coated Ags, and CD19 is required for highly robust responses to such Ag, but it
331 is dispensable for *in vitro* response to soluble Ag[25,27,29,55]. CD19 phosphorylation was robustly
332 induced by anti-IgM and sHEL, but not by pHEL, raising the possibility that CD19 was not
333 engaged by pHEL (**Figure 5C, D**). We therefore generated CD19-deficient MD4 mice to test
334 whether CD19 engagement could account for potent pHEL responses. In contrast to signaling
335 triggered by Ag displayed on a cell membrane or via actin depolymerization[27,29], CD19 is
336 dispensable for robust signaling by particulate Ag *in vitro* **(Figure 5F)**.

337

338 **pHEL trigger robust signal transduction downstream of the BCR by evading LYN-**
339 **dependent inhibitory pathways**

340 PIP3 abundance at the membrane and proximal BCR signaling are both negatively
341 regulated by ITIM domain-containing co-receptors and associated inhibitory phosphatases[48,50].
342 We observed robust phosphorylation of CD22, pSHP1, pSHIP1 in response to anti-IgM and
343 sHEL, but not pHEL (**Figure 5C, D**). This raised the possibility that particulate Ag circumvents
344 engagement of inhibitory coreceptors to drive potent B cell responses. Indeed, exclusion of
345 inhibitory coreceptors and associated phosphatases is postulated to contribute to potent
346 responses by cell membrane-associated Ags[15,20,25,26]. Several Src family kinases (SFK) are
347 expressed in B cells and can all mediate ITAM-dependent signaling downstream of BCR
348 engagement. By contrast, the SFK LYN plays a non-redundant role in phosphorylation of ITIM
349 domains of inhibitory co-receptors; LYN-deficient B cells therefore fail to engage downstream
350 phosphatases SHP1 and SHIP1 in response to anti-IgM stimulation, but can activate ITAM-
351 dependent BCR signaling (as well as CD19) via other SFKs (**Figure 6A**)[48,50,56,57]. To test the
352 hypothesis that pHEL evades engagement of inhibitory co-receptors to trigger highly potent

353 responses – in contrast to soluble stimuli – we generated MD4 B cells deficient for LYN to
354 selectively eliminate all ITIM-dependent signaling. In the absence of LYN, anti-IgM and
355 sHEL-induced pErk and calcium entry were markedly amplified (**Figure 6B-D**). Even sHELT
356 which triggers virtually undetectable pErk in LYN-sufficient B cells exhibit highly enhanced
357 signaling comparable to pHELT (**Supplementary Figure 3A**). By contrast, pHEL responses
358 were not enhanced in MD4.Lyn–/– B cells; no amplification of pHEL signals irrespective of
359 affinity, ED, or dose could be detected in the absence of LYN – even for SVLS with ultralow
360 ED (**Figure 6B-D, Supplementary Figure 3A, B)**. As a result, in MD4.*Lyn*–/– B cells, sHELD
361 and pHELD induced comparably robust pErk and calcium entry **(Figure 6B-D)**, indicating that
362 the evasion of LYN-dependent inhibitory tone by pHEL but not sHEL accounts, at least in part,
363 for the remarkable potency of pHEL in LYN-sufficient B cells. Strikingly, pHEL-induced
364 calcium in MD4 B cells phenocopy the heightened, delayed and prolonged kinetics of calcium
365 responses by LYN-deficient cells to soluble stimuli (**Figure 6D**). Conversely, not only
366 amplitude, but also kinetics of pHEL-induced calcium entry was unaltered by LYN-deficiency
367 (**Figure 6D**). This data further suggests that curtailed signaling triggered by soluble stimuli
368 relative to pHEL was not simply attributable to saturating BCR occupancy and/or
369 internalization of surface receptor as this would not be rescued by LYN-deficiency. Rather we
370 conclude that both signal amplitude and signal duration in response to soluble – but not
371 particulate – Ag is constrained by ITIM engagement.

372

373 **Soluble stimuli dominantly suppress responses to pHEL by engagement of LYN-**
374 **dependent inhibitory pathways**

375 Our data suggests that LYN-dependent inhibitory pathways are engaged and restrain
376 responses to soluble stimuli such as sHEL and anti-IgM, but are evaded by pHEL. We next
377 sought to test whether enforced engagement of LYN-dependent inhibitory pathways by soluble
378 stimuli is sufficient to suppress pHEL signaling. To do so, we developed an assay in which
379 pHEL were pre-bound to MD4 B cells at 4C to forestall signaling, followed by subsequent
380 introduction of soluble stimuli. Cells were then assessed for pErk induction after 20 min
381 incubation at 37C to permit signal transduction. The rationale for this approach is to first ensure
382 BCR engagement by high ED pHEL (which is expected to bind with high avidity). Subsequent
383 introduction of soluble stimuli bound to abundant free BCRs are predicted to dominantly co-
384 engage inhibitory pathways. Importantly, kinetics of signaling by pHEL are not altered by this

385 incubation strategy and still peak at 20 minutes in the absence of sHELD (**Figure 6E** and DNS).
386 By contrast, treatment of pHEL-bound cells with sHEL was sufficient to suppress signaling
387 and this suppression required LYN (**Figure 6E, Supplementary Figure 3C**). Such suppression
388 by sHEL was both affinity- and dose-dependent. Importantly, this suppression was not merely
389 due to competition for receptor binding by sHEL-WT as lower affinity sHELD could also
390 suppress signaling by pre-bound high ED pHELD (**Figure 6E**), as could anti-IgM treatment
391 (which neither engages IgD BCRs nor competes with HEL epitope for binding of the Hy10
392 IgM BCR) (**Supplementary Figure 3C**). In all cases, such suppression was rescued in the
393 absence of LYN (**Figure 6E, Supplementary Figure 3C**).

394 These data suggest that co-ligation with soluble stimuli can prevent signaling by pHEL
395 in a LYN-dependent manner. We next sought to determine whether such soluble stimuli, via
396 LYN engagement could terminate signaling *after* initiation. To do so, we adapted a flow-based
397 calcium assay to trigger cytosolic calcium increases with pHELD and subsequently add either
398 soluble stimulus (or control) once peak of the response is reached (**Figure 6F, G,**
399 **Supplementary Figure 3D**). Indeed, following pHEL stimulation cytosolic calcium remains
400 at maximal levels in a fraction of WT MD4 B cells and this signal is rapidly terminated with
401 addition of soluble stimuli; we found that addition of either anti-IgM or sHELD was sufficient
402 to completely suppress prolonged pHEL calcium responses. Importantly, this was completely
403 LYN-dependent in the case of anti-IgM and partially LYN-dependent for sHELD. These data
404 suggest that signal termination is neither due to displacement of pHEL from BCRs, nor to
405 internalization of BCRs because anti-IgM treatment neither blocks nor removes IgD BCRs
406 from the B cell surface. Rather, we conclude that dominant engagement of LYN-dependent
407 inhibitory signaling by soluble stimuli suppresses B cell responses to particulate Ag.

408

409 **pHEL induces a highly robust NF-κB signal that mimics CD40 stimulation**

410 When comparing differences in signal transduction induced by sHEL and pHEL, we
411 noted that NF-κB activation was disproportionately enhanced by pHEL (**Figure 4A, Figure**
412 **7A**). BCR activation elicited by sHEL or anti-IgM cross-linking only resulted in weak
413 phosphorylation of IKKβ, the catalytic subunit required for its kinase activity and downstream
414 NF-κB translocation to the nucleus[58]. However, IKKβ was highly phosphorylated in response
415 to pHEL **(Figure 7A)** and correspondingly, IκBα (the substrate of IKK catalytic activity) was
416 rapidly and robustly degraded in response to pHEL but not soluble stimuli like sHEL and anti-

417 IgM **(Figure 7B-D)**. As with other signaling nodes interrogated, NF-κB activation was
418 independent of pHEL Ag affinity but sensitive to pHEL ED and concentration **(Figure 7B, E)**.
419 Since the degradation of IκBα is required to release p65 to translocate to the nucleus, we
420 isolated nuclei from stimulated B cells and directly probed for p65 in permeabilized nuclei. In
421 agreement with IKK phosphorylation and IκBα kinetics, we show that p65 is found in high
422 abundance in the nucleus of B cells stimulated with pHEL **(Figure 7F)**.

423 It has been proposed that mature naïve follicular B cells require two signals in order
424 to mount an immune response: signal 1 delivered by the BCR and signal 2 delivered by T cell
425 help, in part via CD40L-CD40 interaction. CD40 is a TNF-receptor superfamily member
426 which strongly activates NF-κB pathway. By contrast, soluble Ag and even anti-IgM cannot
427 trigger comparably robust NF-κB activation at any dose *in vitro* and this may help confer
428 dependence on signal 2. Since pHEL readily drives highly robust NF-κB activation relative to
429 soluble Ag, we hypothesized that Ag displayed on particles of viral size might mimic co-
430 stimulation and bypass the requirement for T cell help. Indeed, immunization with pHEL is
431 sufficient to produce Ab response in the absence of T cell help and without adjuvant (biorxiv
432 preprint 2023)[59]. We therefore stimulated B cells with either sHEL or pHEL in the presence
433 or absence of CD40 ligation. As expected, CD40 stimulation triggered robust IκBα
434 degradation and nuclear translocation of p65 both independently and in combination with
435 soluble BCR stimuli **(Figure 7F, G)**. However, CD40 stimulation produced no additional
436 increase in NF-κB activation when combined with pHEL. Rather, pHEL alone drives IκBα
437 degradation and p65 nuclear accumulation that is comparable in magnitude to that induced by
438 CD40 cross-linking, suggesting that BCR activation by pHEL was sufficient to convey
439 costimulatory-like information. Moreover, pHEL exhibited highly bimodal p65 nuclear
440 translocation in a dose-dependent manner such that even low doses of pHEL induced
441 maximal signal in a subset of cells (**Figure 7F**). Interestingly, unlike for pErk and calcium
442 entry **(Figure 6B-D)**, the genetic absence of LYN was not capable of rescuing the defect in
443 IκB degradation by sHEL, but did so partially in response to anti-IgM (**Figure 7H)**. This
444 observation implies that capacity of pHEL to trigger robust NF-κB activation is not
445 completely accounted for by evasion of inhibitory co-receptor engagement, and that other
446 unique features of dense Ag display on virus-sized particles efficiently link BCR to NF-κB
447 activation. Importantly, IκBα degradation by SVLS was independent of MYD88 (**Figure 7I,**
448 **Supplementary Figure 3E)**.
449

450 **pHEL drive very robust B cell growth, MYC induction, and survival in the absence of co-**
451 **stimulation**

452 We next sought to explore the functional consequences of potent, prolonged, and
453 qualitatively distinct signaling by particulate Ag display. We analyzed downstream cellular
454 outcomes including cell growth, survival, and proliferation. We found that cell growth – as
455 measured by forward scatter by flow cytometry – was greatly enhanced in response to pHEL
456 relative to sHEL after 24 hours **(Figure 8A)**. These data suggested that cell growth induced by
457 particulate Ag could exceed that triggered by maximal soluble Ag stimulation. Because cell
458 growth is associated with cMYC upregulation[60,61], we assayed MYC induction in response to
459 both soluble and particulate stimuli. After 24 hrs, we found that – relative to other markers of
460 B cell activation, including CD69 and CD86 – 1pM pHELT induced higher intra-cellular MYC
461 protein expression than maximally potent doses of sHEL-WT and anti-IgM (**Figure 8B)**. This
462 suggested that qualitatively distinct signaling by pHEL efficiently promotes and sustains MYC
463 protein accumulation. Consistent with this observation, we also found that pHEL promotes
464 cMYC expression disproportionately to NUR77-eGFP upregulation after 24 hr stimulation
465 (**Supplementary Figure 4A).** Consistent with robust NF-κB activation and MYC induction,
466 at successive timepoints in culture we found that B cell survival was consistently enhanced by
467 pHEL relative to sHEL even with addition of the B cell survival factor BAFF **(Figure 8C,**
468 **Supplementary Figure 4B)**. Importantly, neither MYC nor CD69 nor cell growth triggered
469 by pHEL was dependent on MYD88 (**Figure 8D, E, Supplementary Figure 4C**).

470

471 **pHEL reduces the NUR77-eGFP signaling threshold required for B cell proliferation in**
472 **a manner that mimics T cell help**

473 We previously showed that the NUR77-eGFP reporter reveals a sharp T cell receptor
474 signaling threshold required for cell division[62]. Here we show that the reporter reflects an
475 analogous threshold in B cells stimulated through the BCR and this is not altered by dose of
476 anti-IgM, sHEL, or titration of the BTK inhibitor ibrutinib **(Supplementary Figure 4D)**. CD8
477 but not CD4 T cells exhibit a reduction in this threshold in response to IL-2 supplementation,
478 entering cell cycle at lower levels of TCR-induced NUR77-EGFP expression[63]. Similarly,
479 among dividing B cells supplemented with IL-4, the NUR77-eGFP level is markedly reduced
480 **(Supplementary Figure 4E)**. Consistent with the hypothesis that pHEL may mimic co-
481 stimulation, we find that the NUR77 level among dividing B cells stimulated with pHEL (even

482 low density and low affinity) is markedly reduced about 10-fold compared to sHEL **(Figure**
483 **8F, G, Supplementary Figure 4F)**. Because this cannot be reproduced with any dose/affinity
484 of sHEL or anti-IgM stimulation (**Supplementary Figure 4D, F**), this suggests that pHEL is
485 delivering not only a more potent signal to B cells, but a qualitatively distinct one. The addition
486 of IL-4 co-stimulation increases the number of divisions and reduces NUR77 levels among
487 dividing cells responding to sHEL but does not alter the already low GFP expression following
488 pHEL stimulation **(Figures 8F, G)**. This suggests that the pHEL BCR signal alone is sufficient
489 to reduce the NUR77 signaling threshold for B cell proliferation and can mimic this effect of
490 IL-4.

491 We previously reported that C-MYC marks an invariant threshold for proliferation in
492 T cells that is enforced irrespective of co-stimulation[63]**.** Consistent with literature suggesting
493 that MYC also imposes a minimal threshold for B cell proliferation[60,64], we find that both
494 polyclonal and MD4 B cells entering cell division also express an invariant level of MYC, and
495 neither pHEL nor co-stimulation alter this threshold in B cells **(Figure 8H-J, Supplementary**
496 **Figure 4G, H)**. Rather, we postulate that both pHEL and co-stimulatory stimuli – relative to
497 soluble Ag alone – induce and maintain MYC expression to a greater extent relative to NUR77–
498 eGFP, and this is evident as early as 24 hrs before cell division has occurred (**Supplementary**
499 **Figure 4B**). Efficient and sustained induction of MYC relative to NUR77 by pHEL – even in
500 the absence of co-stimulation – may contribute to the T cell-independence of this mode of Ag
501 display. By contrast, soluble Ag stimuli require co-stimulatory second signals to sustain MYC
502 protein expression.

503

504 Discussion

505 Although the assembled BCR complex has recently been visualized via cryo-EM, the
506 mechanism by which Ag triggers signaling continues to be debated[12]. Yet, it remains widely
507 accepted that multivalent Ags induce potent B cell responses by virtue of a high avidity
508 interaction and receptor cross-linking. We reveal that this does not fully explain remarkable
509 sensitivity of B cells to virus-like Ag display. Rather, we show that SVLS triggers signal
510 amplification downstream of the BCR that is due, at least in part, to complete evasion of
511 inhibitory co-receptor engagement but is independent of CD19 (see model, **Supplementary**
512 **Figure 5**). This contrasts with membrane Ags that rely on CD19 for potency, and also with

513 soluble Ags that engage ITIM pathways to curtail signaling and impose tolerance and T cell-
514 dependence.

515 Evasion of inhibitory signaling by particulate Ag lowers the threshold for activation
516 relative to soluble Ag, enabling B cells to sense and respond to μM affinity epitopes.
517 Reducing SVLS dose decreases the fraction of B cells that signal, but the amplitude of
518 response is unaltered. This observation suggests that even a small number of particles with
519 virus-like Ag display may be sufficient to trigger maximal signaling in a single B cell, and
520 implies signal amplification downstream of BCR engagement by particulate Ag. It will be of
521 great interest to rigorously identify the minimal number of SVLS and BCRs required to
522 activate a B cell, and to determine whether signal amplification indeed occurs at the level
523 PIP3 accumulation as biochemical evidence suggests.

524 Many biologically relevant Ags, including particulate Ag, are captured on APCs and
525 presented directly to B cells *in vivo*[31-37]. Ag presented on a cell membrane dramatically
526 reduces the threshold of B cell activation *in vitro*, enabling responses to very low-affinity Ags
527 [20-22] and even to haptens that are non-stimulatory in soluble monovalent form[19]. Nevertheless,
528 B cells can discriminate ligand affinity in this context in part via mechanical pulling forces at
529 the contact interface [14,18,23,24,65]. By contrast, we find no evidence of affinity discrimination to
530 SVLS *in vitro* at the level of any proximal signaling readout assessed (including NF-κB,
531 MAPK, and calcium pathways). Indeed, maximal "all-or-none" responses on a single cell
532 level to virus-like Ag display would be expected to preclude affinity discrimination.
533 Moreover, such discrimination very early in the B cell response to bona fide virus is not
534 merely dispensable, but undesirable[66]. Rather, later capture of virus by FDC to guide affinity
535 maturation in the germinal center is a setting where affinity discrimination of membrane Ag
536 is imperative and occurs[67].

537 Imaging of B cells encountering membrane Ag has previously revealed progressive
538 growth of BCR microclusters at the contact interface which spread and then contract into an
539 immune synapse (IS) in a manner dependent on actin depolymerization. Such membrane re-
540 organization can juxtapose BCRs to co-receptors such as CD19, while inhibitory molecules
541 are excluded from the IS[20,23,27,28]. Indeed, agents that depolymerize actin (to recapitulate such
542 cell surface reorganization) are sufficient to trigger BCR signaling in a manner that is
543 completely dependent upon CD19, IgM BCR, downstream signaling machinery such as
544 PLCγ2, and is also constrained by inhibitory coreceptor CD22[28-30]. CD19 is the signaling

545 component of the CD21/CD81/CD19 complex required to reduce the threshold for B cell
546 activation by complement-coated Ag[55]. Yet, CD19 also has a unique, CD21- and
547 complement-independent role in B cell activation; although it is dispensable for BCR
548 signaling in response to soluble Ag, CD19 is required for sensitizing B cells to cell membrane
549 Ag display[27,29]. Distinct from membrane Ag, CD19 is dispensable for B cell response to
550 particulate Ag suggesting this may not rely on actin dynamics to juxtapose coreceptors and
551 BCRs. However, after particulate Ag is captured and presented on APCs *in vivo*[31-36], B cell
552 response is likely to become highly CD19-dependent both because of membrane-Ag
553 presentation and complement fixation[55].

554 Soluble Ag stimuli are highly constrained by LYN-dependent inhibitory pathways,
555 but we show that SVLS entirely evades LYN-dependent inhibitory tone, resulting not only in
556 heightened amplitude, but also markedly prolonged kinetics of signaling. Exclusion of CD22,
557 FcγRIIb, and SHP1 has been visualized at the IS of B cells interacting with cell membrane-
558 associated Ag, and enforced FcγRIIb engagement is sufficient to prevent BCR clustering in
559 response to membrane Ag[20,25,26]. Yet, it remains to be determined whether these pathways are
560 normally engaged at early time points by membrane Ag. Indeed, CD22 deletion comparably
561 restricts calcium entry triggered by both soluble anti-kappa Ab stimulation and LatA-induced
562 actin depolymerization[30]. LYN-deficient DT40 chicken B cell lines are completely defective
563 in both membrane Ag and LatA responses[28,68], but unlike primary mouse B cells, DT40
564 express predominantly LYN SFK which is required for all ITAM signaling and does not
565 isolate a role for ITIMs. It will be of great interest to define how LYN-dependent ITIM
566 pathways impact membrane Ag signaling in mammalian B cells.

567 Importantly, we show that super-imposed stimulation with soluble antigenic stimuli
568 (anti-IgM or even sHEL) is sufficient to prevent and/or terminate SVLS-induced signaling
569 and this is at least partly LYN-dependent. This shows that forced engagement of LYN-
570 dependent inhibitory signaling pathways can dominantly suppress pHEL responses. One
571 candidate substrate of LYN that may mediate this effect is CD22 which can interact with the
572 IgM BCR in a manner that depends on cis-ligands, and mediates inhibition by recruiting
573 SHP1[48,50,57]. Indeed, engineered expression of CD22 ligands on HEL-conjugated lipid
574 nanoparticles can fully abrogate BCR signaling, suppressing phosphorylation of AKT, CD19,
575 as well as Erk, calcium entry, and IκB degradation[69]. Whether CD22 alone or other ITIM-
576 containing inhibitory co-receptors also account for LYN-dependent suppression of soluble

577 but not SVLS signaling remains to be determined along with the effector PTPases required to
578 do so (SHP-1, SHIP1 or others).
579 How do SVLS evade LYN-dependent inhibitory co-receptor engagement? Mature
580 naïve B cells co-express IgM and IgD BCRs which not only exhibit markedly different
581 abundance on the surface of naïve follicular B cells [30], but may also form separate pre-
582 existing nanoclusters on resting cells prior to Ag encounter[29,70]. Estimates for the size of these
583 nanoclusters (60-240nm)[29,70] overlaps with the diameter of viruses found in nature. Such
584 BCR nanoclusters harbor 30-120 molecules of IgD per cluster (corresponding to 6000-24000/
585 μm^2) and less densely packed IgM at the lower end of this range[29]. We postulate that aligning
586 particle size and spacing of epitopes with that of BCR nanoclusters may maximize BCR
587 engagement while also physically evading inhibitory co-receptor engagement. Indeed,
588 pHELD-HD has 6,000 epitopes per μm^2 which in turn corresponds roughly to 10nm optimal
589 hapten spacing described in the "immunon" model and may trigger maximally potent B cell
590 responses by even a small number of particles[8]. Naturally occurring viruses have epitope
591 densities that range from 200 to 30,000 molecules per μm^2; HIV occupies the lowest end of
592 this spectrum and this may facilitate its immune evasion[39,71]. Capacity to trigger potent
593 signaling across a range of ED may also relate to conformational flexibility of SVLS. Future
594 work could explore whether responses to rigidly structured VLPs and bona fide viral particles
595 share features of SVLS signaling, and whether lipid nanoparticles offer unique advantages as
596 scaffolds for flexible Ag display in vaccine design.

597 IgM and IgD BCRs also differ in sensitivity to different forms of Ag by virtue of
598 distinct flexibility in their hinge regions; Ubelhart et.al suggested that monovalent Ag can
599 signal through IgM but not IgD BCRs, while multivalent Ags can trigger both to signal[72],
600 although Sabouri et al. showed monomeric HEL can engage both[73]. High IgD expression on
601 mature follicular B cells and preserved IgD on anergic B cells that downregulate IgM may
602 sensitize these populations to particulate Ag display by viruses or virus-like particles[41,42].
603 Differential IgM and IgD engagement by soluble and particulate Ag could also contribute to
604 qualitative differences in signaling because IgM and IgD BCRs exhibit different co-receptor
605 association – including CD22 and CD19[17,29,30]. These hypotheses warrant future investigation
606 as does the responsiveness of other BCR isotypes expressed on memory B cells to SVLS.

607 Multivalent Ags – and viral Ag display in particular – can trigger T-independent B
608 cell responses[1]. We show that multivalent Ag display on SVLS – independent of MYD88 or
609 T cell co-stimulation – triggers not only strong MAPK and calcium pathway activation, but

610 also robust NF-κB activation (comparable to that induced by CD40 engagement), sustained
611 MYC expression, as well as enhanced cell growth, survival and proliferation. Highly robust
612 and bimodal NF-κB activation by SVLS may reflect signal amplification downstream of PIP3
613 at the level of BTK dimerization and trans-autophosphorylation (Y322)[53], as well as positive
614 feedback over CARMA1/IKKβ[74]. In addition, strong and prolonged calcium signals can
615 activate IKK[46,75]. Soluble Ag, by contrast, drives much less robust NF-κB activation, triggers
616 apoptosis, and exhibits a much higher NUR77-eGFP threshold for MYC-dependent
617 proliferation, suggesting not only a quantitative but also a qualitative difference in the B cell
618 response to soluble and particulate Ag. MYC is postulated to set an invariant threshold for
619 proliferation (as we observe here)[64], to drive cell growth, and to 'fuel' clonal expansion in the
620 GC by orchestrating a transcriptional program of metabolic remodeling[60,76,77]. Robust and
621 sustained NF-κB and MYC expression may be sufficient to support pHEL-stimulated B cells
622 to grow, survive, and proliferate in the absence of T cell input, and may help explain the
623 molecular basis of T cell-independent B cell responses to multivalent Ags. Importantly,
624 robust responses to SVLS are not restricted to MZ B cells which play critical roles in early
625 response to T-independent multivalent model Ags [44]. Rather, the biology we have uncovered
626 is a general property of naïve, follicular B cells. Consistent with this, T-independent Ab
627 responses are triggered by SVLS administered subcutaneously and without adjuvant *in vivo*
628 in a manner likely to engage lymph node resident follicular B cells [78].

629 Autoreactive BCRs are common in the mature B cell repertoire, and one teleological
630 explanation for their retention is to preserve a reservoir of protective specificities that can
631 respond to cross-reactive viral epitopes under pressure to evolve towards self (near-self
632 hypothesis[79,80]). However, such B cells are constrained by IgM downregulation, dampened
633 signal transduction (anergy), reduced survival, and suppression of CD86 upregulation –
634 mechanisms that prevent the induction of autoimmunity *in vivo*[42,45,47]. Yet self-Ag arrayed on
635 viruses and virus-like particles, including VSV, papillomavirus-like particles, Qβ
636 bacteriophage particles, and lipid nanoparticles can indeed break tolerance[9,78,81-84]. Previous
637 work from us shows that high ED on lipid nanoparticles similar to those used in the present
638 study is sufficient to drive secretion of class-switched IgG *in vivo* in response to self-Ag in
639 the absence of T cell help[78]. How does epitope display on virus-like particles activate anergic
640 B cells even in the absence of co-stimulation? The BCR signaling circuitry that enforces B
641 cell anergy and dependence on "signal 2" (T cell-input) relies on ITIM-dependent inhibitory
642 pathways[50]. We show that pHEL is sufficient to induce maximal calcium entry in a subset of

643 MD4.ML5 anergic B cells and propose that SVLS break tolerance by selective evasion of
644 LYN-dependent inhibitory tone. Differential engagement of such inhibitory tone may
645 represent a fundamental mechanism by which self-reactive naïve B cells can accurately
646 discriminate the same Ag presented in different forms, enabling anergic cells to remain
647 unresponsive in the face of soluble self-Ag until recruited into an immune response by bona
648 fide viral encounter.

649 Together, these molecular insights reveal that density of epitope display on particles
650 of viral size – independent of other viral features like encapsulated nucleic acid – serves as a
651 stand-alone danger signal sufficient to breach B cell anergy by triggering a unique mode of
652 BCR signaling that differs from both typical soluble and membrane Ags. We identify a role
653 for inhibitory coreceptors that confers potency to such particles independent of avidity.
654 Addressed in independent work (biorxiv preprint 2023)[59] is understanding how nucleic acid
655 delivered by SVLS or viruses activate B cells synergistically[85-87]. Our data suggests that
656 mature B cells are intrinsically 'built' as a sensor for virus-like supramolecular structures and
657 poised to mount rapid, potent, and initially T-independent responses to viral threats.

658

659

660

661 Materials and Methods

662 *Mice.* NUR77-EGFP and IgHEL (MD4) mice were previously described[41,42]. C57BL/6 and
663 CD45.1+ BoyJ mice were originally from The Jackson Laboratory. Lyn$^{-/-}$ mice were
664 previously described[56]. MYD88$^{tm1.Defr}$ (Jackson labs #009088) (MYD88$^{-/-}$ herein) encodes a
665 deletion of exon 3 of the myeloid differentiation primary response gene 88 gene[88].
666 Cd19$^{tm1(Cre)Cgn}$ (Jackson labs #006785) (CD19$^{-/-}$ herein) has a Cre recombinase gene inserted
667 into the first exon of the CD19 gene and thus abolishing Cd19 gene function[89]. ML5 mice
668 (Jackson Labs #002599) that expresses sHEL Tg were previously described[42]. All strains were
669 fully backcrossed to the C57BL/6J genetic background for at least 6 generations. Mice were
670 used at 6-9 wk of age for all functional and biochemical experiments. All mice were housed in
671 a specific pathogen-free facility at University of California, San Francisco, according to the
672 University Animal Care Committee and National Institutes of Health (NIH) guidelines.

673

674 *SVLS synthesis and quantification.* All SVLS used throughout this study were prepared
675 following protocols previously described by us[38]. In brief, SVLS were constructed using
676 nonimmunogenic lipids, with phosphatidylcholine and cholesterol comprising ≥ 95% of all
677 lipids. We prepared unilamellar liposomes using a mixture of DSPC, DSPE-PEG maleimide,
678 and cholesterol. Empty liposomes were generated using PBS and extruded membrane with a
679 pore size of 100 nm. Hen egg lysozyme (HEL) recombinant proteins with free engineered
680 cysteines were conjugated to the surface of liposomes via maleimide-thiol chemistry at
681 specific engineered cysteine and programmable epitope density by modulating molar
682 percentage admixed DSPE-PEG maleimide (0.5-5%). A large excess of free cysteines at the
683 end of a 1 h cross-linking reaction to quench all of the available maleimide groups that
684 remain on the liposomal surface. After this conjugation, the liposomes were purified away
685 from free excess HEL proteins by running through a size exclusion column (SEC). Epitope
686 density was quantified using methods that we established previously[38,90] that were also
687 validated by single-molecule fluorescence[91,92]. Control SVLS (pLIP02) had no surface
688 protein conjugation. Recombinant HEL-WT, HEL-D (R73E, D101R), HEL-T (R73E,
689 D101R, R21Q) proteins were overexpressed in *E. coli* and purified to >95% purity following
690 our established protocols[38] and are used throughout except WT HEL from Sigma (1 μg/ml) is
691 used in S2F, 4C, 4D, 7I, and 8B.

692

693 *Antibodies and Reagents.*

694 ***Antibodies for surface markers***: Streptavidin (SA) and antibodies to B220 (RA3-6B2),
695 CD19 (1D3), CD21 (7G6), CD23 (B3B4), CD86 (GL-1), CD69 (H1.2F3), CD45.1 (A20),
696 CD45.2 (104) conjugated to biotin or fluorophores (BioLegend, eBiosciences, BD, or
697 Tonbo).

698 ***Antibodies for intra–cellular staining***: pErk1/2 T202/Y204 mAb (clone 194G2, cat. 4377S)
699 pS6 S235/236 mAb (clone 2F9, cat. 4856S), IκBα Ab (cat. 9242S), NF-κB p65 mAb (clone
700 D14E12, cat. 8242S), C-MYC mAb (clone D84C12, cat. 5605S) were from Cell Signaling
701 Technologies; Donkey anti–rabbit secondary Ab conjugated to APC was from Jackson
702 Immunoresearch.

703 ***Antibodies for immunoblots***: All antibodies except where otherwise noted were from Cell
704 Signaling: C-MYC mAb (clone D84C12), pERK T202/Y204 mAb (clone 197G2, cat.
705 4377S), GAPDH Ab (14C10, cat. 3683s), pCD19 Y531 Ab (cat. 3571S), pSHP-1 Y564 mAb
706 (clone D11G5, cat. 8849S), pSHIP1 Y1020 Ab (cat. 3941S), pPLCγ2 Y1217 Ab (cat. 3871S),
707 pCD79A Y182 Ab (cat. 5173S), pSYK Y525/526 mAb (clone C87C1, cat. 2710S); pBTK
708 Y223 mAb (clone D9T6H, cat. 87141S), pPI3K [p85 Y458, p55 Y199] mAb (clone E3U1H,
709 cat. 17366S), pAKT T308 mAb (clone D25E6, cat. 13038S), pAKT S473 Ab (cat. 9271S),
710 pIKKα/β S176/180 mAb (clone 16A6, cat. 2697S) were from Cell Signaling Technology,
711 anti-phosphotyrosine clone 4G10 was made from a hybridoma and was a gift from the Weiss
712 lab. pCD22 Y822 [mouse Y837] mAb (clone Y506, cat. ab32123) was from Abcam. Anti-
713 mouse- and anti-rabbit- HRP secondary Ab were from Southern Biotech.
714 ***Stimulatory Antibodies and reagents***: Goat anti-mouse IgM F(ab')2 was from Jackson
715 Immunoresearch; Murine IL-4 (10ng/ml , cat#214-14, Peprotech), anti-CD40 (1μg/ml, hm40-
716 3 clone; BD Pharmingen), recombinant murine BAFF (20ng/ml, cat#2106-BF, R&D), LPS
717 (10μg/ml O26:B6; Sigma), CpG (2.5μM ODN 1826; InvivoGen).

718 ***Media:*** Complete culture media was prepared with RPMI-1640 + L-glutamine (Corning-
719 Gibco), Penicillin Streptomycin L-glutamine (Life Technologies), 10 mM HEPES buffer
720 (Life Technologies), 55 mM β-mercaptoethanol (Gibco), I mM sodium pyruvate [(Life
721 Technologies), Non-essential Amino acids (Life Technologies), 10% heat inactivated FBS
722 (Omega Scientific). This was used for all *in vitro* culture and stimulation except for calcium
723 signaling experiments. Calcium flux media was prepared with RPMI, HEPES, PSG as above
724 and 5% FCS.

725 ***Inhibitors***: SYKi (Bay 61-3606 1μM) and PI3Ki (Ly290049 10μM) were from Calbiochem,
726 BTKi (ibrutinib 100nM from Jack Taunton, UCSF), IRAK1/4i (R568 1μM, gift from Rigel)

727 *Flow Cytometry and data analysis*. After staining, cells were analyzed on a Fortessa (Becton
728 Dickinson). Data analysis was performed using FlowJo (v9.9.6 and v10) software (Treestar
729 Inc.). Proliferative indices 'division index' and '% divided' were calculated using FlowJo.
730 Statistical analysis and graphs were generated using Prism v6 (GraphPad Software, Inc).
731 Statistical tests used throughout are listed at the end of each figure legend. Student's paired or
732 unpaired T test (two-tailed and parametric) was used to calculate p values for all comparisons
733 of two pre-specified groups depending on experimental design. ANOVA was performed
734 when more than two groups were compared to one another. Error bars in graphs represent
735 SEM.

736 *Intracellular staining to detect pERK, pS6, IκB, and cMYC.* Following *in vitro* stimulation for
737 varying times, 10^6 cells / well were resuspended in 96-well plates, stained with fixable
738 live/dead dye as above for overnight time points, fixed in 2% paraformaldehyde (PFA) for 10
739 min, washed in FACS buffer, and permeabilized with ice-cold 90% methanol at −20 °C
740 overnight, or for at least 30 minutes on ice. Cells were then washed in FACS buffer, stained
741 with intra-cellular Ab x 45 minutes, washed in FACS buffer, and then stained with Alexa
742 647-conjugated secondary Goat anti-Rabbit antibody along with directly conjugated
743 antibodies to detect surface lineage and/or subset markers for 45 minutes. Samples were
744 washed and then refixed with 2%PFA.

745 *Intracellular Calcium Flux.* Cells were loaded with 5 μg/mL Indo-1 AM per manufacturer's
746 instructions (Life Technologies) and stained with lineage markers B220, CD23, CD21 for 15
747 min. Cells were rested at 37 ºC for 3 min, and Indo-1 fluorescence was measured by FACS
748 immediately prior to and after stimulation to determine intracellular calcium.

749 *Live/dead staining.* LIVE/DEAD Fixable Near-IR Dead Cell Stain kit (Invitrogen). Reagent
750 was reconstituted as per manufacturer's instructions, diluted 1:1000 in PBS, and cells were
751 stained at a concentration of 2×10^6 cells /100μL on ice for 10 min.

752 *Vital dye loading.* Cells were loaded with CellTrace Violet (CTV; Invitrogen) per the
753 manufacturer's instructions except at 5×10^6 cells/ml rather than 1×10^6 cells/ml.

754 *In Vitro B Cell Culture and Stimulation.* Splenocytes or lymphocytes were harvested into
755 single cell suspension through a 40μm cell strainer, subjected to red cell lysis using ACK

756 (ammonium chloride potassium) buffer in the case of splenocytes, +/– CTV loading as
757 described above, and plated at a concentration of 2.5-10 × 10^5 cells/200 µL (depending on
758 assay) in round bottom 96 well plates in complete RPMI media with stimuli for 1-3 days. *In*
759 *vitro* cultured cells were stained to exclude dead cells as above in addition to surface or intra-
760 cellular markers for analysis by flow cytometry depending on assay.

761 *Immunoblot analysis.* Purified splenic/LN B cells (protocol described below) were harvested
762 from mice, pre-warmed for 15 min at 37˚C, and mixed with stimuli in RPMI for 3 min at
763 37˚C. Following stimulation, cells were lysed with 1% NP40 lysis buffer with protease and
764 phosphatase inhibitors for 15 min at 4˚C, and centrifuged for 10 min at 20,000g to remove
765 cellular debris. The supernatants were denatured at 95˚C for 5 min in SDS sample buffer with
766 2.5% β-ME. Lysates were run on Tris-Bis thick gradient (4%-12%) gels (Invitrogen) in
767 MOPS buffer, and transferred to PVDF membranes with a Mini-Protean Tetra cell (Bio-rad).
768 Membranes were blocked for 1 h with 3% BSA TBST, and then probed with primary
769 antibodies listed above, overnight at 4˚C. The next day, membranes were washed three times
770 with TBST for 10 min, and incubated with HRP-conjugated secondary antibodies. Blots were
771 developed utilizing a chemiluminescent substrate (Western Lightning Plus ECL, Perkin
772 Elmer), and visualized with a ChemiDoc Touch Imaging System (Bio Rad). Quantification of
773 western blots was performed with Image Lab Software (Bio Rad).

774 *B cell purification.* B cell purification was performed utilizing MACS separation per
775 manufacturer's instructions. In short, pooled spleen and/or lymph nodes were prepared
776 utilizing the B cell isolation kit (Miltenyi), and purified by negative selection through an LS
777 column (Miltenyi).

778 *Nuclei isolation / nuclear staining.* The nuclei isolation protocol was based on previously
779 published report[93].

780 *Nuclei isolation*. In brief, purified splenic/LN B cells (protocol described below) were
781 harvested from mice and pre-warmed in a 96-well plate for 10 min at 37°C with
782 1.5x10^6cells/100 µl per well in complete media (RPMI with 10% FBS, penicillin,
783 streptomycin, glutamine, HEPES, β-ME, sodium pyruvate, and non-essential amino acids).
784 Cells were stimulated with 100 µl of 2x stimuli for 20 min at 37°C. Stimulated cells were
785 spun at 300 x *g* and 4°C, and the pellets were immediately resuspended with 250 µl of ice-
786 cold Buffer A containing 320 mM sucrose, 10 mM HEPES (Life Technologies), 8 mM
787 $MgCl_2$, 1× Roche EDTA-free complete Protease Inhibitor, and 0.1% (v/v) Triton X-100

788 (Sigma-Aldrich). After 15 min on ice, the plate was spun at 2000 × *g* and 4°C for 5 min. This
789 was followed by two 250 µl washes with Buffer B (Buffer A without Triton X-100) and
790 spinning at 2000 × *g* and 4°C for 5 min. After the final wash, pellets were resuspended with
791 200 µl Buffer B containing 4% paraformaldehyde (electron microscopy grade; Electron
792 Microscopy Sciences), and nuclei were rested on ice for 30 min for fixation. The nuclei were
793 spun at 2000 x *g* and 4°C for 5 min, and followed by two washes and resuspension in FACS
794 Buffer (1× PBS with 2% FBS and 8mM $MgCl_2$), centrifuging at 1000 × *g* and 4°C for 5 min
795 to sufficiently pellet nuclei.

796 *Nuclei staining*. Isolated nuclei were washed with 200 µl Perm Buffer (FACS Buffer with
797 0.3% Triton-X 100) and spun at 1000 × *g* and 4°C for 5 min. Isolated nuclei were stained
798 with 50 µl purified rabbit anti-mouse NF-κB p65 (Cell Signaling 8242S) diluted (1:100) in
799 Perm Buffer for 30 min on ice. The 96-well plate was spun at 1000 x *g* and 4°C for 5 min,
800 and washed with 200 µl FACS Buffer. The nuclei were then stained with 50 µl anti-rabbit
801 IgG-APC (Jackson Immunoresearch, 711-136-152) diluted (1:100) in Perm Buffer for 30 min
802 on ice in the dark. The nuclei were spun at 1000 x *g* and 4°C for 5 min, and washed with 200
803 µl FACS Buffer. Nuclei were resuspended in 200 µl FACS Buffer and analyzed immediately
804 on a BD Fortessa cytometer.

805

806 Acknowledgments

807 We thank our funders – R01AI155653 (WC, JZ), NIAID R01AI148487 (JZ), NIAMS
808 R01AR069520 (JZ), NIAID AAI Postdoctoral Fellowship (JFB and JZ), NIH Training Grant
809 T32 AI007334 (JR). We thank Dr. Arthur Weiss for helpful discussions and critical reading
810 of the manuscript. We thank Al Roque for help with mouse husbandry.

811

812 Declaration of interest

813 JZ serves as a scientific consultant for Walking Fish Therapeutics. WC has a patent pending
814 on SVLS. The authors have no other declarations.

References

1 Bachmann, M. F. & Zinkernagel, R. M. Neutralizing antiviral B cell responses. *Annu Rev Immunol* **15**, 235-270, doi:10.1146/annurev.immunol.15.1.235 (1997).

2 Feldmann, M. & Easten, A. The relationship between antigenic structure and the requirement for thymus-derived cells in the immune response. *J Exp Med* **134**, 103-119 (1971).

3 Abbott, R. K., Lee, J. H., Menis, S., Skog, P., Rossi, M., Ota, T., . . . Crotty, S. Precursor Frequency and Affinity Determine B Cell Competitive Fitness in Germinal Centers, Tested with Germline-Targeting HIV Vaccine Immunogens. *Immunity* **48**, 133-146 e136, doi:10.1016/j.immuni.2017.11.023 (2018).

4 Kato, Y., Abbott, R. K., Freeman, B. L., Haupt, S., Groschel, B., Silva, M., . . . Crotty, S. Multifaceted Effects of Antigen Valency on B Cell Response Composition and Differentiation In Vivo. *Immunity*, doi:10.1016/j.immuni.2020.08.001 (2020).

5 Dosenovic, P., Kara, E. E., Pettersson, A. K., McGuire, A. T., Gray, M., Hartweger, H., . . . Nussenzweig, M. C. Anti-HIV-1 B cell responses are dependent on B cell precursor frequency and antigen-binding affinity. *Proc Natl Acad Sci U S A* **115**, 4743-4748, doi:10.1073/pnas.1803457115 (2018).

6 Desaymard, C. & Feldmann, M. Role of epitope density in the induction of immunity and tolerance with thymus-independent antigens. I. Studies with 2,4-dinitrophenyl conjugates in vitro. *Eur J Immunol* **5**, 537-541, doi:10.1002/eji.1830050806 (1975).

7 Desaymard, C. & Howard, J. G. Role of epitope density in the induction of immunity and tolerance with thymus-independent antigens. II. Studies with 2,4-dinitrophenyl conjugates in vivo. *Eur J Immunol* **5**, 541-545, doi:10.1002/eji.1830050807 (1975).

8 Dintzis, H. M., Dintzis, R. Z. & Vogelstein, B. Molecular determinants of immunogenicity: the immunon model of immune response. *Proc Natl Acad Sci U S A* **73**, 3671-3675 (1976).

9 Bachmann, M. F., Rohrer, U. H., Kundig, T. M., Burki, K., Hengartner, H. & Zinkernagel, R. M. The influence of antigen organization on B cell responsiveness. *Science* **262**, 1448-1451 (1993).

10 Zabel, F., Kundig, T. M. & Bachmann, M. F. Virus-induced humoral immunity: on how B cell responses are initiated. *Curr Opin Virol* **3**, 357-362, doi:10.1016/j.coviro.2013.05.004 (2013).

11 Ingale, J., Stano, A., Guenaga, J., Sharma, S. K., Nemazee, D., Zwick, M. B. & Wyatt, R. T. High-Density Array of Well-Ordered HIV-1 Spikes on Synthetic Liposomal Nanoparticles Efficiently Activate B Cells. *Cell Rep* **15**, 1986-1999, doi:10.1016/j.celrep.2016.04.078 (2016).

12 Tolar, P. & Pierce, S. K. Unveiling the B cell receptor structure. *Science* **377**, 819-820, doi:10.1126/science.add8065 (2022).

13 Veneziano, R., Moyer, T. J., Stone, M. B., Wamhoff, E. C., Read, B. J., Mukherjee, S., . . . Bathe, M. Role of nanoscale antigen organization on B-cell activation probed using DNA origami. *Nat Nanotechnol* **15**, 716-723, doi:10.1038/s41565-020-0719-0 (2020).

14 Pierce, S. K. & Liu, W. The tipping points in the initiation of B cell signalling: how small changes make big differences. *Nat Rev Immunol* **10**, 767-777, doi:10.1038/nri2853 (2010).

15 Mattila, P. K., Batista, F. D. & Treanor, B. Dynamics of the actin cytoskeleton mediates receptor cross talk: An emerging concept in tuning receptor signaling. *J Cell Biol* **212**, 267-280, doi:10.1083/jcb.201504137 (2016).

16 Tolar, P. Cytoskeletal control of B cell responses to antigens. *Nat Rev Immunol* **17**, 621-634, doi:10.1038/nri.2017.67 (2017).

17 Gold, M. R. & Reth, M. G. Antigen Receptor Function in the Context of the Nanoscale Organization of the B Cell Membrane. *Annu Rev Immunol* **37**, 97-123, doi:10.1146/annurev-immunol-042718-041704 (2019).

18 Kwak, K., Akkaya, M. & Pierce, S. K. B cell signaling in context. *Nat Immunol* **20**, 963-969, doi:10.1038/s41590-019-0427-9 (2019).

19 Tolar, P., Hanna, J., Krueger, P. D. & Pierce, S. K. The constant region of the membrane immunoglobulin mediates B cell-receptor clustering and signaling in response to membrane antigens. *Immunity* **30**, 44-55, doi:10.1016/j.immuni.2008.11.007 (2009).
20 Batista, F. D., Iber, D. & Neuberger, M. S. B cells acquire antigen from target cells after synapse formation. *Nature* **411**, 489-494, doi:10.1038/35078099 (2001).
21 Batista, F. D. & Neuberger, M. S. B cells extract and present immobilized antigen: implications for affinity discrimination. *EMBO J* **19**, 513-520, doi:10.1093/emboj/19.4.513 (2000).
22 Batista, F. D. & Neuberger, M. S. Affinity dependence of the B cell response to antigen: a threshold, a ceiling, and the importance of off-rate. *Immunity* **8**, 751-759, doi:10.1016/s1074-7613(00)80580-4 (1998).
23 Fleire, S. J., Goldman, J. P., Carrasco, Y. R., Weber, M., Bray, D. & Batista, F. D. B cell ligand discrimination through a spreading and contraction response. *Science* **312**, 738-741, doi:10.1126/science.1123940 (2006).
24 Liu, W., Meckel, T., Tolar, P., Sohn, H. W. & Pierce, S. K. Antigen affinity discrimination is an intrinsic function of the B cell receptor. *J Exp Med* **207**, 1095-1111, doi:10.1084/jem.20092123 (2010).
25 Ambegaonkar, A. A., Kwak, K., Sohn, H., Manzella-Lapeira, J., Brzostowski, J. & Pierce, S. K. Expression of inhibitory receptors by B cells in chronic human infectious diseases restricts responses to membrane-associated antigens. *Sci Adv* **6**, eaba6493, doi:10.1126/sciadv.aba6493 (2020).
26 Sohn, H. W., Pierce, S. K. & Tzeng, S. J. Live cell imaging reveals that the inhibitory FcgammaRIIB destabilizes B cell receptor membrane-lipid interactions and blocks immune synapse formation. *J Immunol* **180**, 793-799, doi:10.4049/jimmunol.180.2.793 (2008).
27 Depoil, D., Fleire, S., Treanor, B. L., Weber, M., Harwood, N. E., Marchbank, K. L., . . . Batista, F. D. CD19 is essential for B cell activation by promoting B cell receptor-antigen microcluster formation in response to membrane-bound ligand. *Nat Immunol* **9**, 63-72, doi:10.1038/ni1547 (2008).
28 Treanor, B., Depoil, D., Gonzalez-Granja, A., Barral, P., Weber, M., Dushek, O., . . . Batista, F. D. The membrane skeleton controls diffusion dynamics and signaling through the B cell receptor. *Immunity* **32**, 187-199, doi:10.1016/j.immuni.2009.12.005 (2010).
29 Mattila, P. K., Feest, C., Depoil, D., Treanor, B., Montaner, B., Otipoby, K. L., . . . Batista, F. D. The actin and tetraspanin networks organize receptor nanoclusters to regulate B cell receptor-mediated signaling. *Immunity* **38**, 461-474, doi:10.1016/j.immuni.2012.11.019 (2013).
30 Gasparrini, F., Feest, C., Bruckbauer, A., Mattila, P. K., Muller, J., Nitschke, L., . . . Batista, F. D. Nanoscale organization and dynamics of the siglec CD22 cooperate with the cytoskeleton in restraining BCR signalling. *EMBO J* **35**, 258-280, doi:10.15252/embj.201593027 (2016).
31 Carrasco, Y. R. & Batista, F. D. B cells acquire particulate antigen in a macrophage-rich area at the boundary between the follicle and the subcapsular sinus of the lymph node. *Immunity* **27**, 160-171, doi:10.1016/j.immuni.2007.06.007 (2007).
32 Pape, K. A., Catron, D. M., Itano, A. A. & Jenkins, M. K. The humoral immune response is initiated in lymph nodes by B cells that acquire soluble antigen directly in the follicles. *Immunity* **26**, 491-502, doi:10.1016/j.immuni.2007.02.011 (2007).
33 Aung, A., Cui, A., Maiorino, L., Amini, A. P., Gregory, J. R., Bukenya, M., . . . Irvine, D. J. Low protease activity in B cell follicles promotes retention of intact antigens after immunization. *Science* **379**, eabn8934, doi:10.1126/science.abn8934 (2023).
34 Junt, T., Moseman, E. A., Iannacone, M., Massberg, S., Lang, P. A., Boes, M., . . . von Andrian, U. H. Subcapsular sinus macrophages in lymph nodes clear lymph-borne viruses and present them to antiviral B cells. *Nature* **450**, 110-114, doi:10.1038/nature06287 (2007).

35 Gonzalez, S. F., Degn, S. E., Pitcher, L. A., Woodruff, M., Heesters, B. A. & Carroll, M. C. Trafficking of B cell antigen in lymph nodes. *Annu Rev Immunol* **29**, 215-233, doi:10.1146/annurev-immunol-031210-101255 (2011).
36 Phan, T. G., Grigorova, I., Okada, T. & Cyster, J. G. Subcapsular encounter and complement-dependent transport of immune complexes by lymph node B cells. *Nat Immunol* **8**, 992-1000, doi:10.1038/ni1494 (2007).
37 Cyster, J. G. B cell follicles and antigen encounters of the third kind. *Nat Immunol* **11**, 989-996, doi:10.1038/ni.1946 (2010).
38 Wholey, W. Y., Mueller, J. L., Tan, C., Brooks, J. F., Zikherman, J. & Cheng, W. Synthetic Liposomal Mimics of Biological Viruses for the Study of Immune Responses to Infection and Vaccination. *Bioconjug Chem* **31**, 685-697, doi:10.1021/acs.bioconjchem.9b00825 (2020).
39 Cheng, W. The Density Code for the Development of a Vaccine? *J Pharm Sci* **105**, 3223-3232, doi:10.1016/j.xphs.2016.07.020 (2016).
40 Paus, D., Phan, T. G., Chan, T. D., Gardam, S., Basten, A. & Brink, R. Antigen recognition strength regulates the choice between extrafollicular plasma cell and germinal center B cell differentiation. *J Exp Med* **203**, 1081-1091, doi:10.1084/jem.20060087 (2006).
41 Zikherman, J., Parameswaran, R. & Weiss, A. Endogenous antigen tunes the responsiveness of naive B cells but not T cells. *Nature* **489**, 160-164, doi:10.1038/nature11311 (2012).
42 Goodnow, C. C., Crosbie, J., Adelstein, S., Lavoie, T. B., Smith-Gill, S. J., Brink, R. a., . . . Raphael, K. Altered immunoglobulin expression and functional silencing of self-reactive B lymphocytes in transgenic mice. *Nature* **334**, 676-682, doi:10.1038/334676a0 (1988).
43 Tan, C., Hiwa, R., Mueller, J. L., Vykunta, V., Hibiya, K., Noviski, M., . . . Zikherman, J. NR4A nuclear receptors restrain B cell responses to antigen when second signals are absent or limiting. *Nature Immunology* **21**, 1267-1279, doi:10.1038/s41590-020-0765-7 (2020).
44 Martin, F. & Kearney, J. F. Marginal-zone B cells. *Nat Rev Immunol* **2**, 323-335, doi:10.1038/nri799 (2002).
45 Tan, C., Noviski, M., Huizar, J. & Zikherman, J. Self-reactivity on a spectrum: A sliding scale of peripheral B cell tolerance. *Immunol Rev* **292**, 37-60, doi:10.1111/imr.12818 (2019).
46 Dolmetsch, R. E., Lewis, R. S., Goodnow, C. C. & Healy, J. I. Differential activation of transcription factors induced by Ca2+ response amplitude and duration. *Nature* **386**, 855-858, doi:10.1038/386855a0 (1997).
47 Healy, J. I., Dolmetsch, R. E., Timmerman, L. A., Cyster, J. G., Thomas, M. L., Crabtree, G. R., . . . Goodnow, C. C. Different nuclear signals are activated by the B cell receptor during positive versus negative signaling. *Immunity* **6**, 419-428, doi:10.1016/s1074-7613(00)80285-x (1997).
48 Dal Porto, J. M., Gauld, S. B., Merrell, K. T., Mills, D., Pugh-Bernard, A. E. & Cambier, J. B cell antigen receptor signaling 101. *Mol Immunol* **41**, 599-613, doi:10.1016/j.molimm.2004.04.008 (2004).
49 Humphries, L. A., Dangelmaier, C., Sommer, K., Kipp, K., Kato, R. M., Griffith, N., . . . Rawlings, D. J. Tec kinases mediate sustained calcium influx via site-specific tyrosine phosphorylation of the phospholipase Cgamma Src homology 2-Src homology 3 linker. *J Biol Chem* **279**, 37651-37661, doi:10.1074/jbc.M311985200 (2004).
50 Getahun, A. Role of inhibitory signaling in peripheral B cell tolerance. *Immunol Rev* **307**, 27-42, doi:10.1111/imr.13070 (2022).
51 Stokoe, D., Stephens, L. R., Copeland, T., Gaffney, P. R., Reese, C. B., Painter, G. F., . . . Hawkins, P. T. Dual role of phosphatidylinositol-3,4,5-trisphosphate in the activation of protein kinase B. *Science* **277**, 567-570, doi:10.1126/science.277.5325.567 (1997).
52 Alessi, D. R., James, S. R., Downes, C. P., Holmes, A. B., Gaffney, P. R., Reese, C. B. & Cohen, P. Characterization of a 3-phosphoinositide-dependent protein kinase which phosphorylates and activates protein kinase Balpha. *Curr Biol* **7**, 261-269, doi:10.1016/s0960-9822(06)00122-9 (1997).

53 Chung, J. K., Nocka, L. M., Decker, A., Wang, Q., Kadlecek, T. A., Weiss, A., . . . Groves, J. T. Switch-like activation of Bruton's tyrosine kinase by membrane-mediated dimerization. *Proc Natl Acad Sci U S A* **116**, 10798-10803, doi:10.1073/pnas.1819309116 (2019).
54 Rawlings, D. J., Scharenberg, A. M., Park, H., Wahl, M. I., Lin, S., Kato, R. M., . . . Kinet, J. P. Activation of BTK by a phosphorylation mechanism initiated by SRC family kinases. *Science* **271**, 822-825, doi:10.1126/science.271.5250.822 (1996).
55 Fearon, D. T. & Carroll, M. C. Regulation of B lymphocyte responses to foreign and self-antigens by the CD19/CD21 complex. *Annu Rev Immunol* **18**, 393-422, doi:10.1146/annurev.immunol.18.1.393 (2000).
56 Chan, V. W., Meng, F., Soriano, P., DeFranco, A. L. & Lowell, C. A. Characterization of the B lymphocyte populations in Lyn-deficient mice and the role of Lyn in signal initiation and down-regulation. *Immunity* **7**, 69-81, doi:10.1016/s1074-7613(00)80511-7 (1997).
57 Xu, Y., Harder, K. W., Huntington, N. D., Hibbs, M. L. & Tarlinton, D. M. Lyn tyrosine kinase: accentuating the positive and the negative. *Immunity* **22**, 9-18, doi:10.1016/j.immuni.2004.12.004 (2005).
58 Shinohara, H. & Kurosaki, T. Comprehending the complex connection between PKCbeta, TAK1, and IKK in BCR signaling. *Immunol Rev* **232**, 300-318, doi:10.1111/j.1600-065X.2009.00836.x (2009).
59 Wholey, W.-Y., Meyer, A. R., Yoda, S.-T., Chackerian, B., Zikherman, J. & Cheng, W. Mechanisms of neutralizing antibody response probed using synthetic virus-like structures. preprint at *bioRxiv*, doi:10.1101/2023.02.20.529089 (2023).
60 Finkin, S., Hartweger, H., Oliveira, T. Y., Kara, E. E. & Nussenzweig, M. C. Protein Amounts of the MYC Transcription Factor Determine Germinal Center B Cell Division Capacity. *Immunity* **51**, 324-336 e325, doi:10.1016/j.immuni.2019.06.013 (2019).
61 Iritani, B. M. & Eisenman, R. N. c-Myc enhances protein synthesis and cell size during B lymphocyte development. *Proc Natl Acad Sci U S A* **96**, 13180-13185, doi:10.1073/pnas.96.23.13180 (1999).
62 Au-Yeung, B. B., Zikherman, J., Mueller, J. L., Ashouri, J. F., Matloubian, M., Cheng, D. A., . . . Weiss, A. A sharp T-cell antigen receptor signaling threshold for T-cell proliferation. *Proc Natl Acad Sci U S A* **111**, E3679-3688, doi:10.1073/pnas.1413726111 (2014).
63 Au-Yeung, B. B., Smith, G. A., Mueller, J. L., Heyn, C. S., Jaszczak, R. G., Weiss, A. & Zikherman, J. IL-2 Modulates the TCR Signaling Threshold for CD8 but Not CD4 T Cell Proliferation on a Single-Cell Level. *J Immunol* **198**, 2445-2456, doi:10.4049/jimmunol.1601453 (2017).
64 Heinzel, S., Binh Giang, T., Kan, A., Marchingo, J. M., Lye, B. K., Corcoran, L. M. & Hodgkin, P. D. A Myc-dependent division timer complements a cell-death timer to regulate T cell and B cell responses. *Nat Immunol* **18**, 96-103, doi:10.1038/ni.3598 (2017).
65 Natkanski, E., Lee, W. Y., Mistry, B., Casal, A., Molloy, J. E. & Tolar, P. B cells use mechanical energy to discriminate antigen affinities. *Science* **340**, 1587-1590, doi:10.1126/science.1237572 (2013).
66 Kalinke, U., Bucher, E. M., Ernst, B., Oxenius, A., Roost, H. P., Geley, S., . . . Hengartner, H. The role of somatic mutation in the generation of the protective humoral immune response against vesicular stomatitis virus. *Immunity* **5**, 639-652, doi:10.1016/s1074-7613(00)80277-0 (1996).
67 Nowosad, C. R., Spillane, K. M. & Tolar, P. Germinal center B cells recognize antigen through a specialized immune synapse architecture. *Nat Immunol* **17**, 870-877, doi:10.1038/ni.3458 (2016).
68 Weber, M., Treanor, B., Depoil, D., Shinohara, H., Harwood, N. E., Hikida, M., . . . Batista, F. D. Phospholipase C-gamma2 and Vav cooperate within signaling microclusters to propagate B cell spreading in response to membrane-bound antigen. *J Exp Med* **205**, 853-868, doi:10.1084/jem.20072619 (2008).

69 Macauley, M. S., Pfrengle, F., Rademacher, C., Nycholat, C. M., Gale, A. J., von Drygalski, A. & Paulson, J. C. Antigenic liposomes displaying CD22 ligands induce antigen-specific B cell apoptosis. *J Clin Invest* **123**, 3074-3083, doi:10.1172/JCI69187 (2013).
70 Maity, P. C., Blount, A., Jumaa, H., Ronneberger, O., Lillemeier, B. F. & Reth, M. B cell antigen receptors of the IgM and IgD classes are clustered in different protein islands that are altered during B cell activation. *Sci Signal* **8**, ra93, doi:10.1126/scisignal.2005887 (2015).
71 Klein, J. S. & Bjorkman, P. J. Few and far between: how HIV may be evading antibody avidity. *PLoS Pathog* **6**, e1000908, doi:10.1371/journal.ppat.1000908 (2010).
72 Ubelhart, R., Hug, E., Bach, M. P., Wossning, T., Duhren-von Minden, M., Horn, A. H., . . . Jumaa, H. Responsiveness of B cells is regulated by the hinge region of IgD. *Nat Immunol* **16**, 534-543, doi:10.1038/ni.3141 (2015).
73 Sabouri, Z., Perotti, S., Spierings, E., Humburg, P., Yabas, M., Bergmann, H., . . . Goodnow, C. C. IgD attenuates the IgM-induced anergy response in transitional and mature B cells. *Nat Commun* **7**, 13381, doi:10.1038/ncomms13381 (2016).
74 Shinohara, H., Behar, M., Inoue, K., Hiroshima, M., Yasuda, T., Nagashima, T., . . . Okada-Hatakeyama, M. Positive feedback within a kinase signaling complex functions as a switch mechanism for NF-kappaB activation. *Science* **344**, 760-764, doi:10.1126/science.1250020 (2014).
75 Berry, C. T., May, M. J. & Freedman, B. D. STIM- and Orai-mediated calcium entry controls NF-kappaB activity and function in lymphocytes. *Cell Calcium* **74**, 131-143, doi:10.1016/j.ceca.2018.07.003 (2018).
76 Calado, D. P., Sasaki, Y., Godinho, S. A., Pellerin, A., Kochert, K., Sleckman, B. P., . . . Rajewsky, K. The cell-cycle regulator c-Myc is essential for the formation and maintenance of germinal centers. *Nat Immunol* **13**, 1092-1100, doi:10.1038/ni.2418 (2012).
77 Dominguez-Sola, D., Victora, G. D., Ying, C. Y., Phan, R. T., Saito, M., Nussenzweig, M. C. & Dalla-Favera, R. The proto-oncogene MYC is required for selection in the germinal center and cyclic reentry. *Nat Immunol* **13**, 1083-1091, doi:10.1038/ni.2428 (2012).
78 Chen, Z., Wholey, W. Y., Hassani Najafabadi, A., Moon, J. J., Grigorova, I., Chackerian, B. & Cheng, W. Self-Antigens Displayed on Liposomal Nanoparticles above a Threshold of Epitope Density Elicit Class-Switched Autoreactive Antibodies Independent of T Cell Help. *J Immunol* **204**, 335-347, doi:10.4049/jimmunol.1801677 (2020).
79 Cancro, M. P. & Kearney, J. F. B cell positive selection: road map to the primary repertoire? *J Immunol* **173**, 15-19, doi:10.4049/jimmunol.173.1.15 (2004).
80 Forsdyke, D. R. Two signal half-century: From negative selection of self-reactivity to positive selection of near-self-reactivity. *Scand J Immunol* **89**, e12746, doi:10.1111/sji.12746 (2019).
81 Chackerian, B., Durfee, M. R. & Schiller, J. T. Virus-like display of a neo-self antigen reverses B cell anergy in a B cell receptor transgenic mouse model. *J Immunol* **180**, 5816-5825 (2008).
82 Chackerian, B., Lenz, P., Lowy, D. R. & Schiller, J. T. Determinants of autoantibody induction by conjugated papillomavirus virus-like particles. *J Immunol* **169**, 6120-6126 (2002).
83 Chackerian, B., Lowy, D. R. & Schiller, J. T. Induction of autoantibodies to mouse CCR5 with recombinant papillomavirus particles. *Proc Natl Acad Sci U S A* **96**, 2373-2378 (1999).
84 Chackerian, B., Lowy, D. R. & Schiller, J. T. Conjugation of a self-antigen to papillomavirus-like particles allows for efficient induction of protective autoantibodies. *J Clin Invest* **108**, 415-423, doi:10.1172/JCI11849 (2001).
85 Rawlings, D. J., Schwartz, M. A., Jackson, S. W. & Meyer-Bahlburg, A. Integration of B cell responses through Toll-like receptors and antigen receptors. *Nat Rev Immunol* **12**, 282-294, doi:10.1038/nri3190 (2012).
86 Hou, B., Saudan, P., Ott, G., Wheeler, M. L., Ji, M., Kuzmich, L., . . . DeFranco, A. L. Selective utilization of Toll-like receptor and MyD88 signaling in B cells for enhancement of the antiviral germinal center response. *Immunity* **34**, 375-384, doi:10.1016/j.immuni.2011.01.011 (2011).

87 Eckl-Dorna, J. & Batista, F. D. BCR-mediated uptake of antigen linked to TLR9 ligand stimulates B-cell proliferation and antigen-specific plasma cell formation. *Blood* **113**, 3969-3977, doi:10.1182/blood-2008-10-185421 (2009).
88 Hou, B., Reizis, B. & DeFranco, A. L. Toll-like receptors activate innate and adaptive immunity by using dendritic cell-intrinsic and -extrinsic mechanisms. *Immunity* **29**, 272-282, doi:10.1016/j.immuni.2008.05.016 (2008).
89 Rickert, R. C., Roes, J. & Rajewsky, K. B lymphocyte-specific, Cre-mediated mutagenesis in mice. *Nucleic Acids Res* **25**, 1317-1318, doi:10.1093/nar/25.6.1317 (1997).
90 Wholey, W. Y., Yoda, S. T. & Cheng, W. Site-Specific and Stable Conjugation of the SARS-CoV-2 Receptor-Binding Domain to Liposomes in the Absence of Any Other Adjuvants Elicits Potent Neutralizing Antibodies in BALB/c Mice. *Bioconjug Chem* **32**, 2497-2506, doi:10.1021/acs.bioconjchem.1c00463 (2021).
91 DeSantis, M. C., Kim, J. H., Song, H., Klasse, P. J. & Cheng, W. Quantitative Correlation between Infectivity and Gp120 Density on HIV-1 Virions Revealed by Optical Trapping Virometry. *J Biol Chem* **291**, 13088-13097, doi:10.1074/jbc.M116.729210 (2016).
92 Pang, Y., Song, H., Kim, J. H., Hou, X. & Cheng, W. Optical trapping of individual human immunodeficiency viruses in culture fluid reveals heterogeneity with single-molecule resolution. *Nat Nanotechnol* **9**, 624-630, doi:10.1038/nnano.2014.140 (2014).
93 Gallagher, M. P., Conley, J. M. & Berg, L. J. Peptide Antigen Concentration Modulates Digital NFAT1 Activation in Primary Mouse Naive CD8(+) T Cells as Measured by Flow Cytometry of Isolated Cell Nuclei. *Immunohorizons* **2**, 208-215, doi:10.4049/immunohorizons.1800032 (2018).

Figure 1. Synthetic virus-like structures (SVLS) induce highly potent B cell responses that depend on epitope density but not affinity.

A. Library of synthetic viral-like structures (SVLS) assembled by conjugated lipid nanoparticles of viral size (120nm) via maleimide chemistry to engineered cysteines in hen egg lysozyme (HEL) affinity mutants at varying epitope density, ED (see also S1B for quantification). **B.** MD4 lymphocytes expressing NUR77-eGFP BAC Tg reporter were stimulated with native soluble HEL (sHEL-WT) or the affinity mutants sHELD and sHELT at varying doses for 24 hrs. GFP expression was analysed by flow cytometry in B220+ B cells and MFI is plotted. Curves fit a three-parameter non-linear regression against the mean of 3 biological replicates per stimulus and EC50 values correspond to these curves (left). EC50 values were also interpolated for individual biological replicates and compared by parametric t-test (right). **C.** Pooled splenocytes and lymphocytes from NUR77-GFP reporter MD4 mice were stimulated with either soluble HELD (sHELD) or SVLS carrying 286 HELD epitopes (pHELD) and analysed 24 hrs later as in B. Data from a representative experiment (left panel) were fitted with a three-parameter non-linear regression. Shaded bar corresponds to equipotent doses of sHELD (1 μg/ml) and pHELD (1pM ~ 4ng/ml HEL). EC50 values were interpolated from 4-5 biological replicates and compared by parametric t-test (right panel). **D.** As in C, but MD4 reporter B cells were stimulated with soluble HELT (sHELT) and SVLS carrying 256 HELT epitopes (pHELT). **E.** As in C, but MD4 reporter B cells were stimulated with titrated densities of HELD per particle. **F.** pHELT and pHELD curves from C, D are overlaid on the same plot (left). EC50 values [μg/ml] HEL protein were interpolated from 4 biological replicates and compared by parametric t-test (right panel). Data in C-F are representative of 7 independent experiments. **G.** MD4 lymphocytes were loaded with CTV vital dye and cultured with soluble HEL stimuli (sHELT, sHELD, sHEL-WT; 3.16 μg/ml and 10-fold dilutions x 4) together with 20 ng/ml BAFF. Representative histograms depict CTV dilution in live B220+ cells after 72 hours (Left). Graphs depict % divided and division index calculated with Flowjo software for 3 biological replicates (right). Groups were compared by parametric two-way ANOVA with Tukey's. **H.** MD4 lymph node cells were loaded with CTV vital dye and cultured with either sHELD/T 1 μg/ml, 0.05 μg/ml or pHELT/D with high or low ED (pHELD-HD = 286, pHELT-HD = 256, pHELD-LD = 61, pHELT-LD = 64) at 1pM or 0.1pM. Representative histograms depict CTV dilution in live B220+ cells after 72 hours. Inset triangles denote high and low dilution of stimulus. Inset arrowheads mark a small fraction of highly proliferative B cells. Histograms are representative of 7 independent experiments.

Figure 1. Synthetic virus-like structures (SVLS) induce very potent B cell responses that depend on epitope density but not affinity

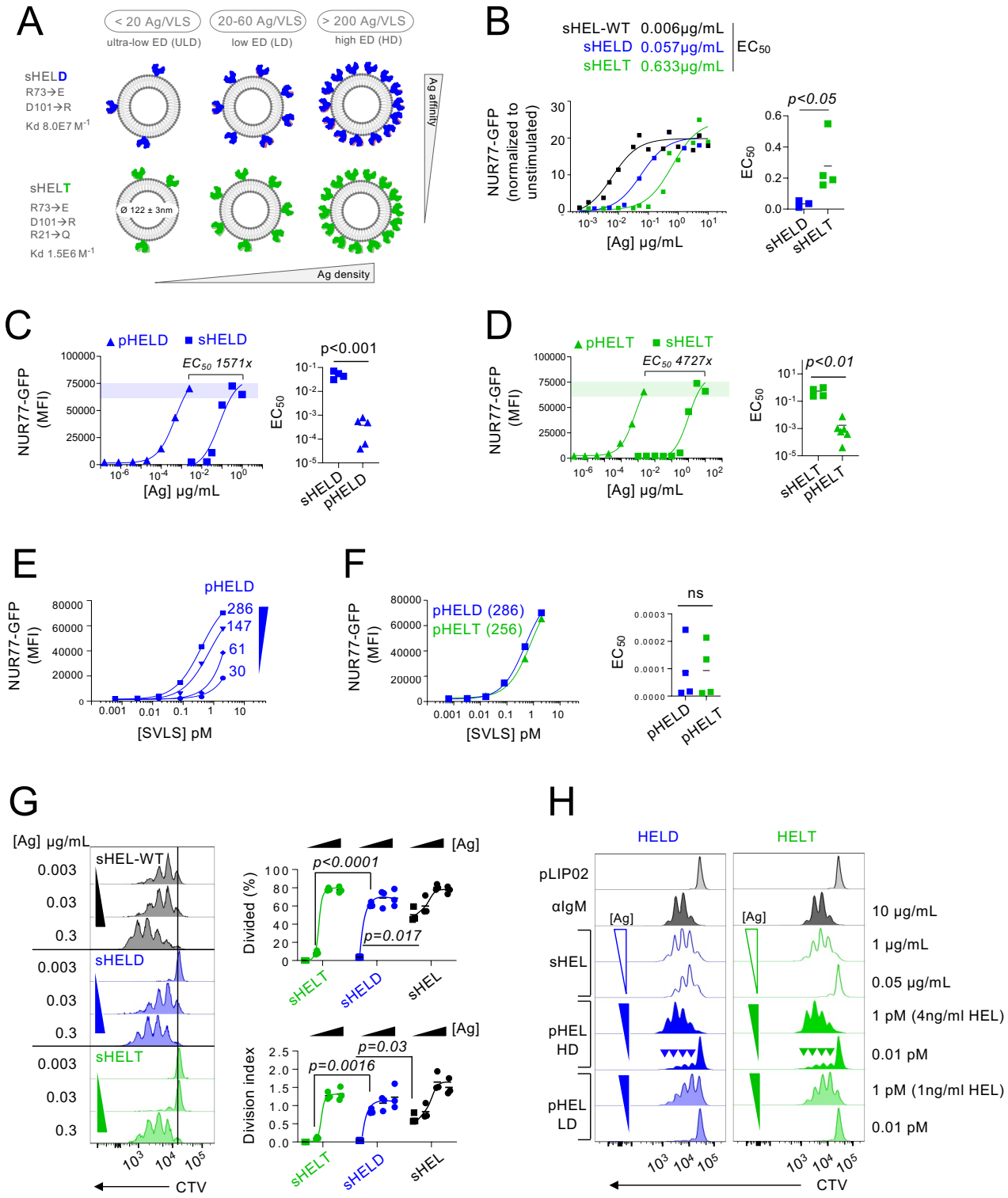

Figure 2. pHEL trigger robust signaling downstream of the BCR that is insensitive to epitope affinity.

A, B. MD4 splenocytes were stimulated over a time course of 120 minutes, fixed, permeabilized, and intra-cellular pErk was measured by flow cytometry (left). Stimuli were pLIP02 = naked liposome 10pM, anti-IgM 10 μg/ml, pHELT or pHELD (256, 286 ED respectively) 1pM [liposome] ≅ 4ng/ml [HEL protein], and sHELT or sHELD 1 μg/ml. Doses of sHEL and pHEL selected were equipotent for induction of NUR77-eGFP at 24 hrs (see Fig 1C, D). Graphs (left) and histograms (right) depict pErk in B220+ cells from a single time course and is representative of 3 independent experiments. **C.** Graph depicts B cell pErk MFI after 20 min stimulation; each point represents an independent experiment and data are pooled from 18 (pHELD) or 8 (pHELT) experiments depending on stimulus. Separate groups are depicted in a single graph for convenience. Pre-specified groups were compared by a paired parametric T-test. **D.** As in A, B, but splenocytes were stimulated with decreasing concentrations of either pHELT or pHELD for 20 min. Data plotted is from a single experiment, representative of >= 4 independent experiments. **E, F.** Splenocytes and lymphocytes from MD4 mice were pooled, loaded with Indo-1 calcium indicator dye, stained to detect B220+ B cells, and stimulated as in A. Calcium entry was detected in real time by flow cytometric detection of bound and unbound Indo-1 fluorescence for 2-10 minutes. Ratio of bound/unbound fluorescence over time is plotted as population mean or for individual cells (F). Data are representative of at least 8 independent experiments.

Figure 2. pHEL trigger robust signal transduction downstream of the BCR that is insensitive to epitope affinity

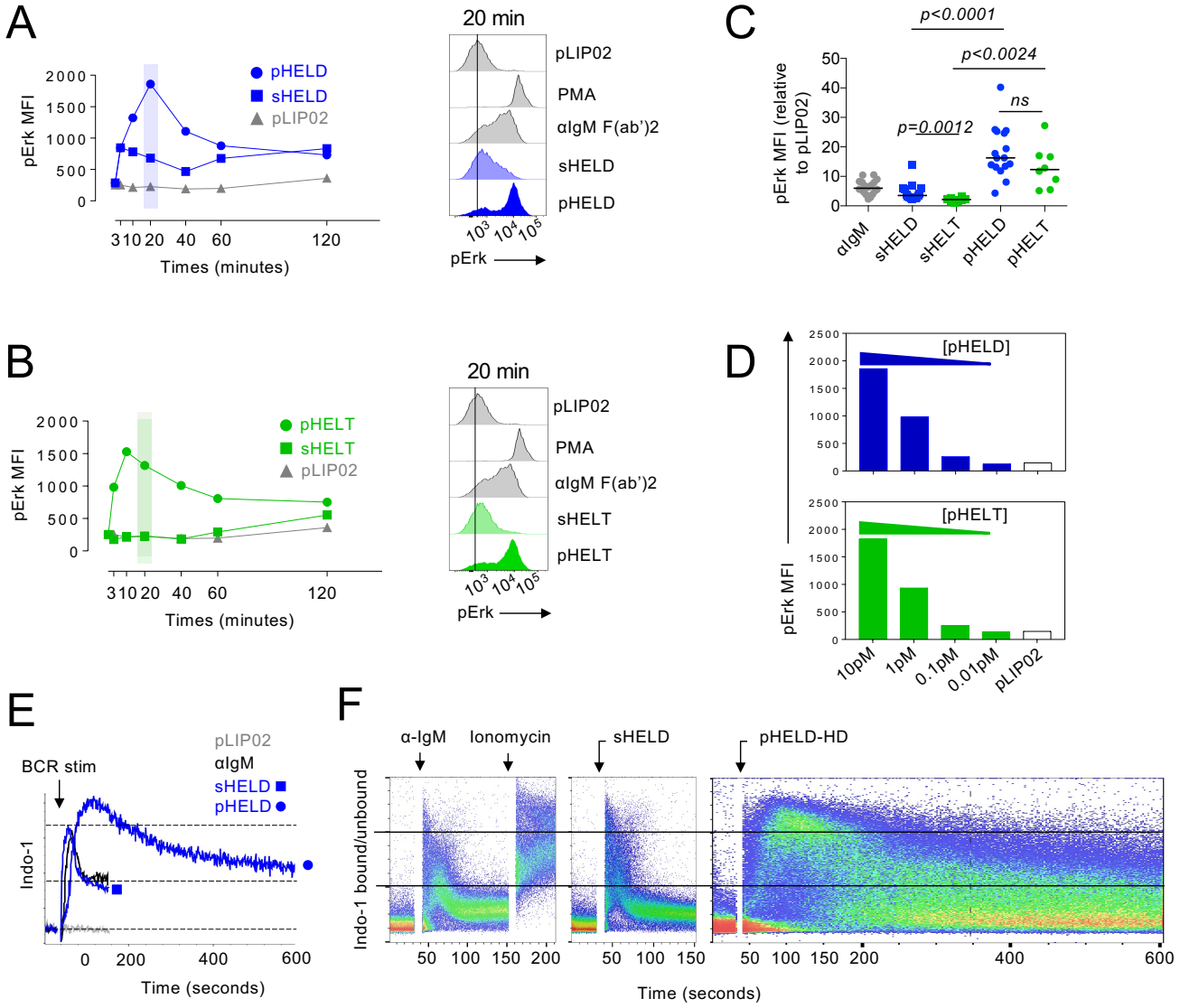

Figure 3. Particulate Ag trigger bimodal signaling that is sensitive to dose and epitope density, but not to epitope affinity.

A. As in 2A/B, but splenocytes were stimulated with decreasing concentrations of either pHELT or pHELD (10pM, 1pM, 0.1pM). Samples correspond to MFI quantification in 2D. Inset goal posts gate on subset of cells with maximal pErk signal. **B.** As in A, but splenocytes were stimulated with 10pM of SVLS carrying either high density (HD) or low density (LD) of HELD or HELT (286, 256, 61, 64 respective ED). Data in A, B is representative of at least 4 independent experiments. **C-E.** Pooled splenocytes and lymphocytes from MD4 mice were loaded with Indo-1 calcium indicator dye, stained with surface markers to detect B220+ cells and in C stimulated with sHELD/T (1 and 0.1 μg/ml). In D cells are stimulated with 1pM or 0.1pM of high or low density pHELD (286, 23 ED respectively), and in E are stimulated with high or low density pHELD/T (286/256, 61/64 ED respectively). Calcium entry was assessed by flow cytometry for indicated time. Plots depict geometric mean of Indo1 bound/unbound fluorescence ratio in individual cells over time (seconds) on a log scale. Histograms display Indo1 bound/unbound fluorescence ratio gated on a defined time window to capture peak cytosolic calcium for each type of stimulus. Data in C-E depict same Indo-1 axis/scale and dashed black line marks corresponding value across dot plots and histograms for comparison. Data are representative of at least 3 independent experiments depending on stimuli. **F, G**. As in 2E, F and 3C except cells from MD4 or MD4.ML5 mice were stimulated with indicated reagents: anti-IgM 10 μg/ml, sHELD 1 μg/ml, or pHELD-HD (ED 286) 1pM. Indo-1 ratio is shown on a linear scale. Gated in G are corresponding time gates to capture fraction of responding or non-responding B cells. Data are representative of 2 independent experiments.

Figure 3. pHEL trigger bimodal signaling that is sensitive to dose and epitope density, but not to epitope affinity

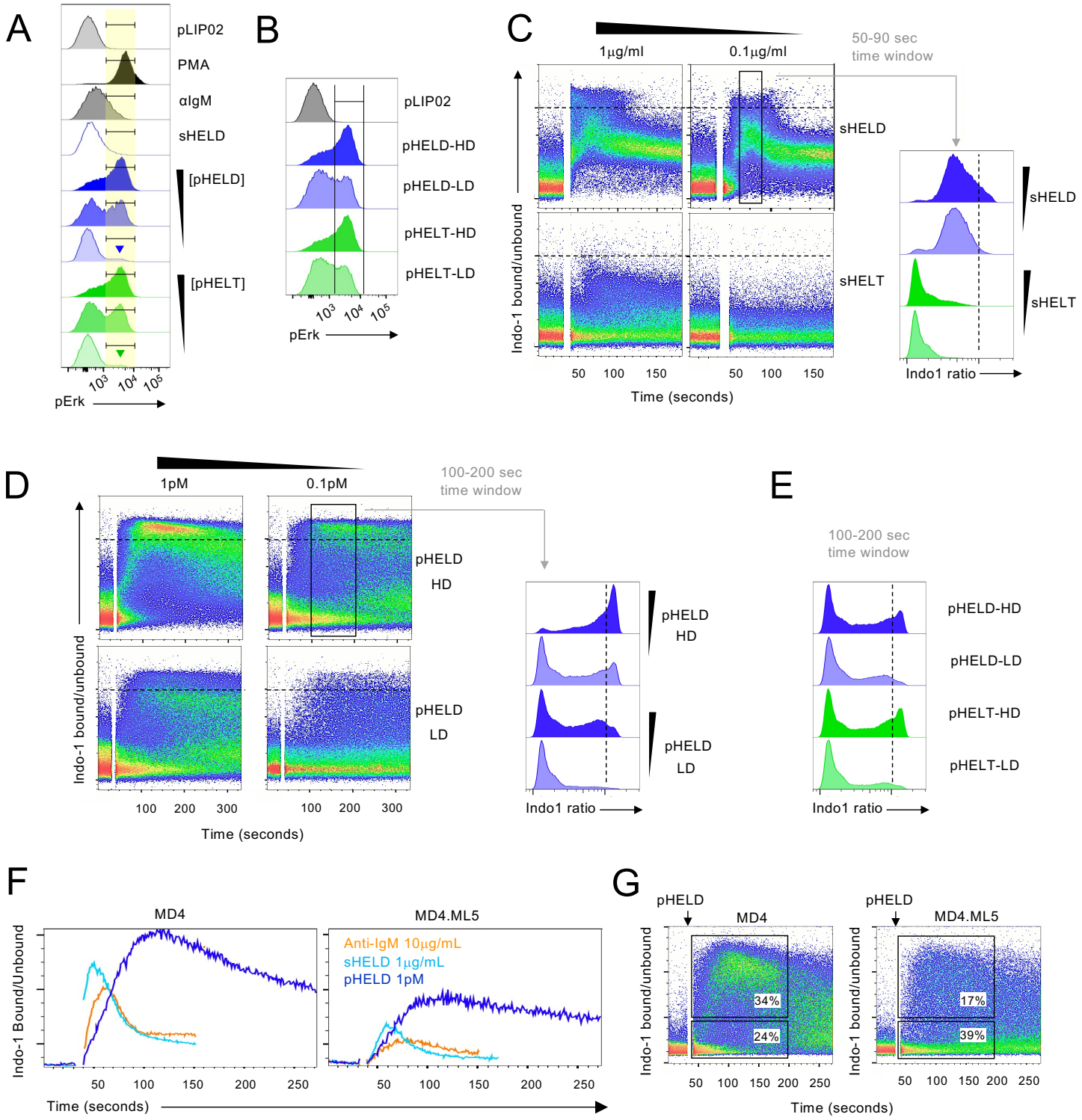

Figure 4. pHEL signaling is independent of MYD88/IRAK1/2 but requires canonical BCR pathway

A, B. Pooled splenocytes and lymphocytes from MD4 mice were pre-incubated at 37C for 15 min with Rigel R568 IRAK1/4 inhibitor (1 μM) followed by 20 min incubation with indicated stimuli (2.5 μM CpG, 1pM pHELD) and then fixed, permeabilized, and stained to detect pErk or pS6 as well as B220. Representative histograms depict pErk (A) or pS6 (B) in B220+ B cells. Graph depicts pErk MFI from 3 independent experiments. Data in B is representative of at least 4 independent experiments. **C, D.** Pooled splenocytes and lymphocytes from MD4 *Myd88*+/+ and MD4 *Myd88*–/– mice were stimulated with indicated stimuli for 20 minutes and stained to detect pErk or pS6 in B220+ B cells as in A, B (LPS 10 μg/ml, CpG 2.5 μM, anti-IgM 10 μg/ml, anti-CD40 1 μg/ml, sHEL-WT 1 μg/ml, or pHELT-HD (ED 256) 1pM,). Histograms depict pErk (C) or pS6 (D) and are representative of 4 (C) or 3 (D) independent experiments. **E, F.** As in 4A except pre-treatment with SYKi (Bay 61-3606 1 μM) or BTKi (ibrutinib 100mM), followed by 20 minute incubation with indicated stimuli: pHELD-HD (ED 286) 1pM and 0.1pM (F), sHELD 1 μg/ml, anti-IgM 10 μg/ml, 2.5 μM CpG. Histograms are representative of 4 independent experiments. **G, H.** As in 4A except pre-treatment with PI3Ki (Ly290049 10 μM) and stimuli (pHELT-HD ED=256 1pM in G; pHELD-LD ED=53 and pHELT-LD ED=58 1pM in H). Histograms are representative of at least 4 independent experiments.

Figure 4. pHEL signaling is independent of MYD88 and IRAK1/4 but requires canonical BCR pathway

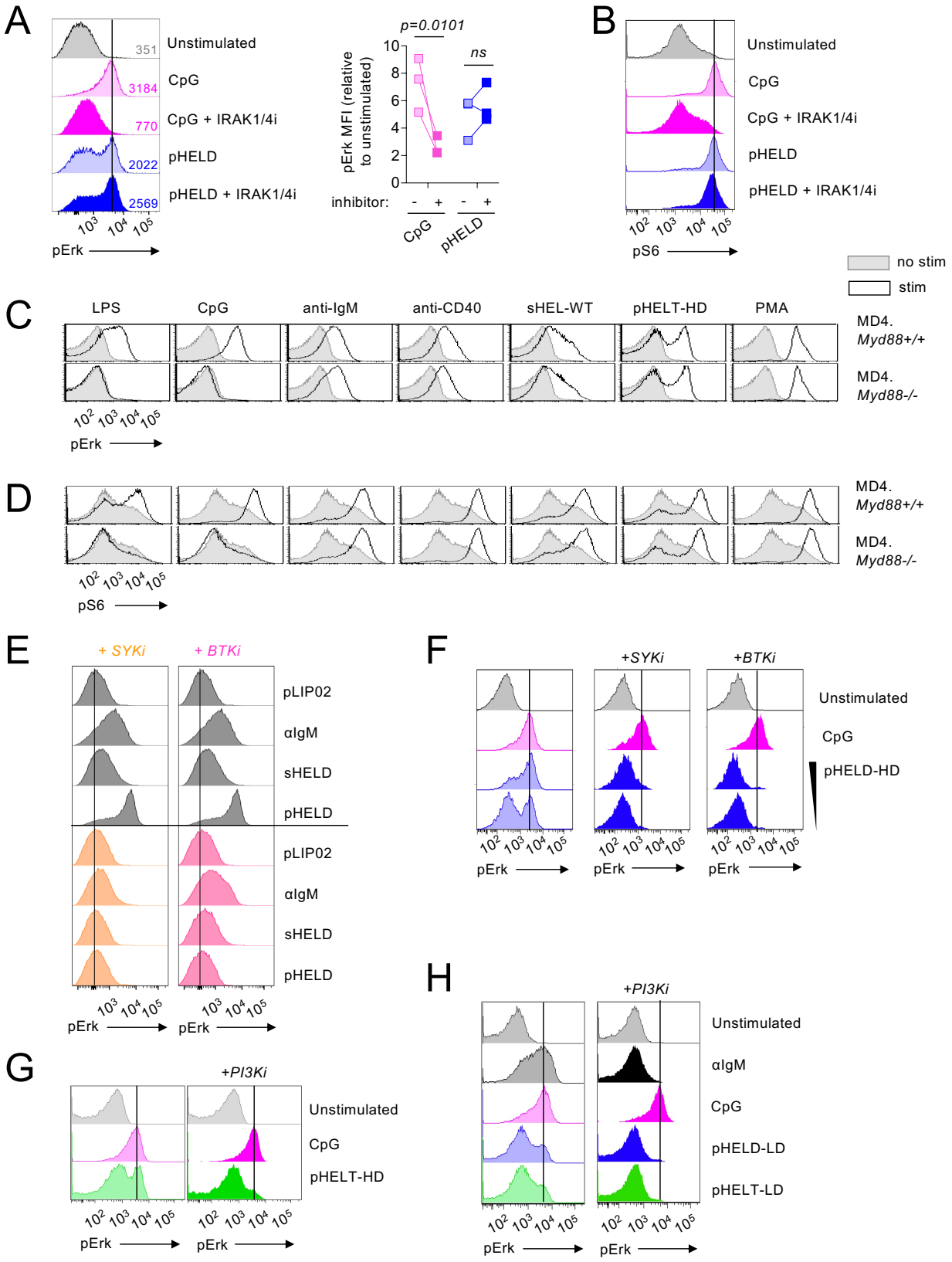

Figure 5. pHEL trigger robust signal amplification downstream of the BCR

A-C. MD4 splenocytes and lymphocytes were pooled, and B cells were isolated by bench-top negative selection. B cells were stimulated for 3 min at 37C with either naked liposome (pLIP02 1pM), 10 μg/ml anti-IgM, 1 μg/ml sHEL-WT / sHELD, or 1pM pHELD / pHELT (high ED 250-290). Lysates were analysed by western blotting to detect total phospho-tyrosine (4G10) or specific phospho-species in the BCR signaling cascade. GAPDH (panel B and C, bottom) is shown as a loading control because a common pool of cells was used for all stimulation conditions. Images depict blots performed with a single set of lysates representative of 3-6 independent experiments depending on blotting Ab with corresponding quantification across biological replicates in D, E. **D, E.** Summary data of phosphoprotein quantification from 3-4 independent experiments. Quantification shows raw band intensity without normalization. Rather, in each experiment, blots were probed for GAPDH as depicted in B to confirm accurate loading. Error bars depict SEM. **F.** 20' Phosflow assay to detect pErk in *Cd19*+/– or *Cd19*–/– MD4 splenocytes after stimulation with either control pLIP02 1pM, 10 μg/ml anti-IgM, 1 μg/ml sHELD, or 1pM pHELD-HD. Samples were co-stained with B220, CD23, and CD21 to detect B cell subsets. Histograms depict CD23+ B cells and are representative of 4 independent experiments.

Figure 5. pHEL trigger robust signal amplification downstream of the BCR

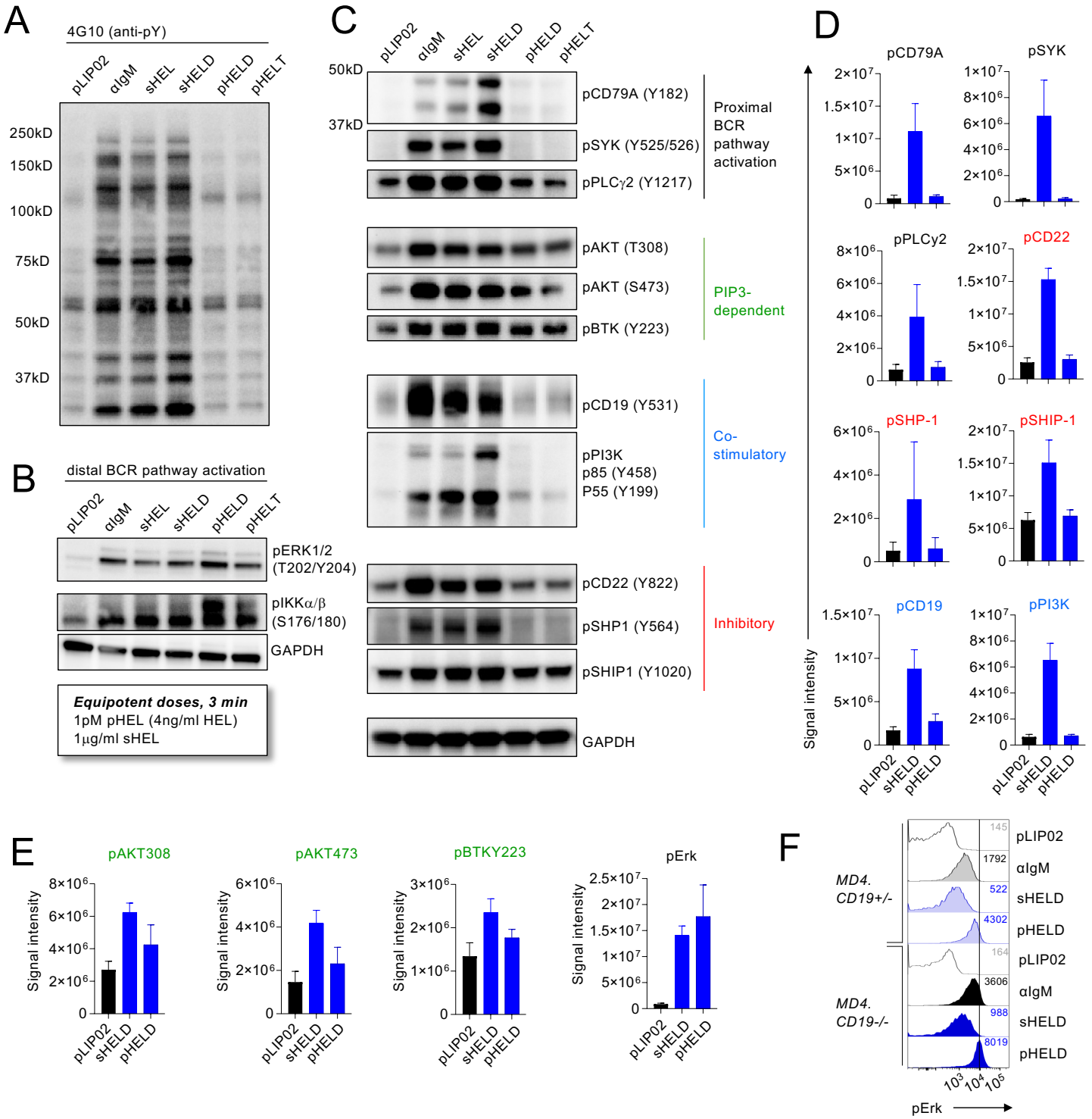

Figure 6. Soluble but not particulate Ag are restrained by LYN-dependent inhibitory signaling

A. Lysates were generated and probed as in 5A-C, except either WT or *Lyn*–/– polyclonal B cells were stimulated for 3 minutes with 10 μg/ml anti-IgM. Blot is representative of at least 3 independent experiments. **B.** 20' Phosflow assay to detect pErk in *Lyn*+/+ and *Lyn*–/– MD4 pooled splenocytes and lymphocytes after stimulation with either control pLIP02 1pM, 10 μg/ml anti-IgM, 1 μg/ml sHELD, or pHELD. Both high density and low density (HD/LD 286, 61) pHELD were used at two doses each (1, 0.1pM). Samples were co-stained with B220, CD23, and CD21 to detect B cell subsets. Inset values represent MFI. Histograms depict CD23+ B cells and are representative of at least 8 independent experiments. **C.** Graph depicts data in B pooled from 3-4 independent experiments. Pre-specified groups were compared by parametric T-tests and are plotted together on the same graph for convenience. **D.** Pooled splenocytes and lymphocytes from *Lyn*+/+ and *Lyn*–/– MD4 mice were loaded with Indo-1 calcium indicator dye, stained with CD21 and CD23 surface markers to detect B220+ subsets, and stimulated with anti-IgM (10 μg/ml), sHELD (1 μg/ml), or pHELD-HD (ED 289, 1pM). Calcium entry was assessed by flow cytometry for indicated time as in 2E, F. Plots depict geometric mean of Indo1 bound/unbound fluorescence ratio over time in CD23+ B cells (seconds). Data are representative of 3 independent experiments. **E.** Splenocytes from *Lyn*+/+ and *Lyn*–/– MD4 mice were incubated with 1st stimulus at 4C for 15 minutes, followed by 2nd add-in stimulus (or media) for another 15 min at 4C. Cells were then incubated for 20' at 37C, and fixed, permeabilized, and stained as in 2A to detect pErk. 1st stimuli: 10 μg/ml anti-IgM, 1 μg/ml sHELD, or 5pM pHELD-HD (ED 289). 2nd add-in doses of sHEL-WT or sHELD as annotated (μg/ml). histograms depict B220+ cells and are representative of 4 independent experiments. **F, G.** As in D except with late addition of 10μg/ml anti-IgM following pHEL stimulation at indicated time (gray kinetic curve). Data in F depict geometric mean of Indo1 bound/unbound fluorescence ratio over time in CD23+ B cells, while F depicts same samples with single cell reslution. Data are representative of at least 3 independent experiments.

Figure 6. Soluble but not particulate Ag are restrained by LYN-dependent inhibitory signaling

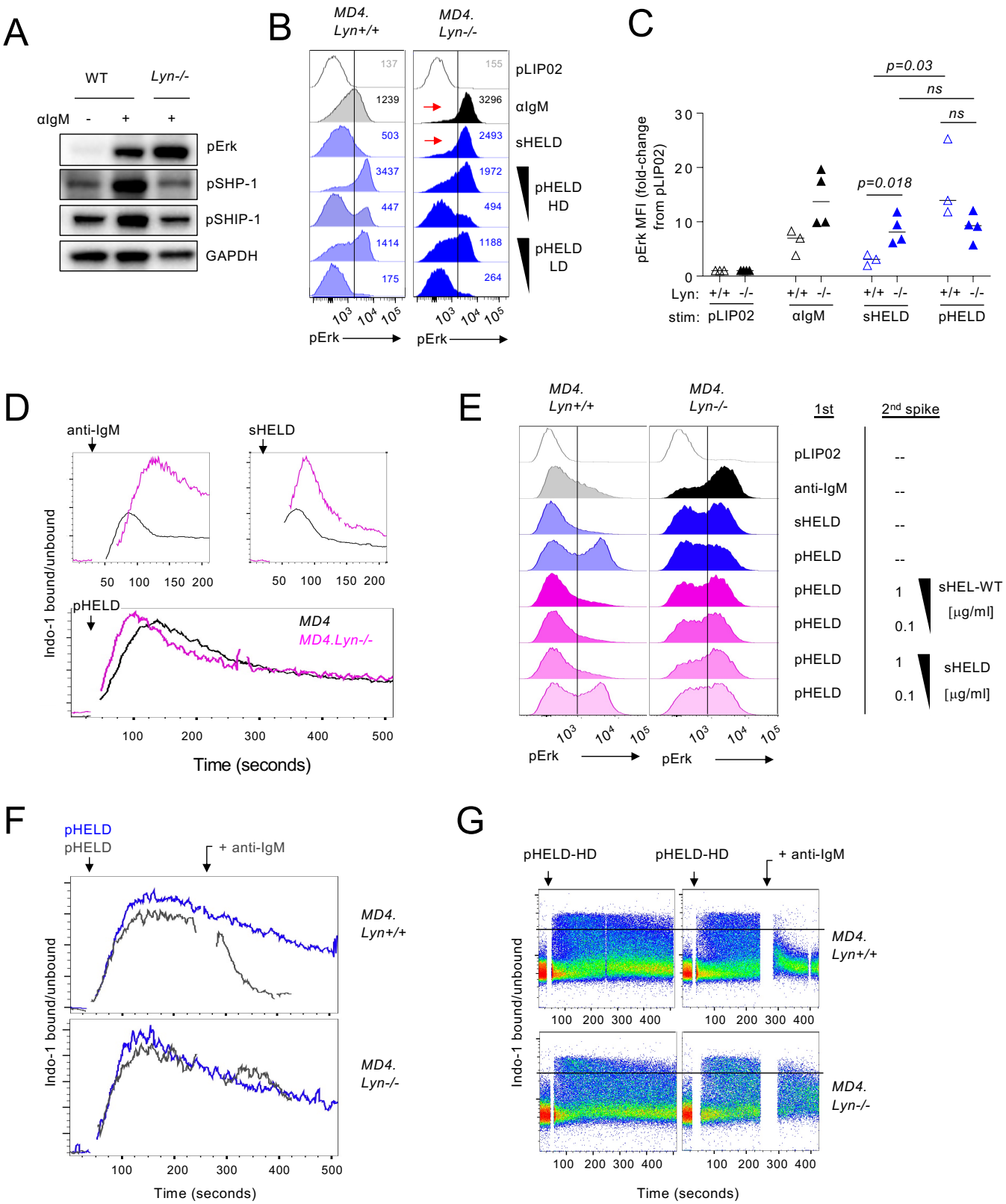

Figure 7. pHEL trigger highly robust NF-κB signaling that mimics co-stimulation and is independent of MYD88.

A. Lysates were prepared as in Fig 5 but probed for pIKKα/β and pErk as shown in 5B. Western blot images are representative of 4 independent experiments. Quantification (right) show raw band intensity for IKKα and IKKβ subunits, error bars show SEM. **B-D.** As in Fig 2A/B, pooled splenocytes and lymphocytes from MD4 mice were stimulated over a time course, fixed, permeabilized, and stained to detect total intra-cellular IκBα by flow cytometry. Graph (B) depicts IκB MFI in B220+ cells at 20 minutes. Each data point represents an individual experiment pooled from >=8 independent experiments. Groups were compared by a parametric T-test. Stimulation with either sHELD/pHELD-HD (C) or sHELT/pHELT-HD (D) is shown across a time course (left) and representative histograms (right) depict IκB degradation in B220+ cells after 20 minutes. **E.** As in B-D except histograms showing IκBα degradation at 20 minutes post-stimulation for soluble stimuli sHELD/T and pHELT/D with high or low ED (HD vs. LD). Inset triangles represent decreasing concentration of pHEL (10, 1, 0.1pM). Data are representative of >= 4 independent experiments. **F.** B cells were isolated by negative selection from MD4 spleen and lymph nodes. Cells were stimulated for 20 minutes (10ug/ml anti-IgM, 0.1, 1, 10pM pHELT-HD, 1μg/ml sHEL-WT +/- 1 μg/ml anti-CD40), and nuclei were purified by centrifugation against a density gradient. Nuclei were then permeabilized and stained. Nuclei were gated based on FSC and SSC as shown in representative plot (left) and interrogated for nuclear translocated p65 (right). Data are representative of 3 independent experiments. **G.** Purified B cells were stimulated in the presence or absence of anti-CD40 (1 μg/ml) as well as sHEL 1 μg/ml or pHEL 1pM, and IκBα degradation was measured by intracellular staining 20 minutes later. Each overlaid histogram shows internal negative control pLIP02 as reference (dotted histogram). Light shaded histograms show BCR stimulus condition alone, dark shaded histograms show BCR stimulus condition + anti-CD40. Data are representative of >= 3 independent experiments. **H.** As in 6B, except splenocytes from *Lyn*+/+ and *Lyn*–/– MD4 mice were stained to detect intracellular IκB in CD23+ B cells at 20 minutes. Data are representative of 3 independent experiments. **I.** As in 4C, D except stained to detect intracellular IκB in CD23+ B cells at 20 minutes. Data are representative of 3 independent experiments. In panels C, D, E, H, I: line in offset histograms references internal negative control.

Figure 7. pHEL trigger highly robust NF-κB signaling that mimics co-stimulation and is independent of MYD88

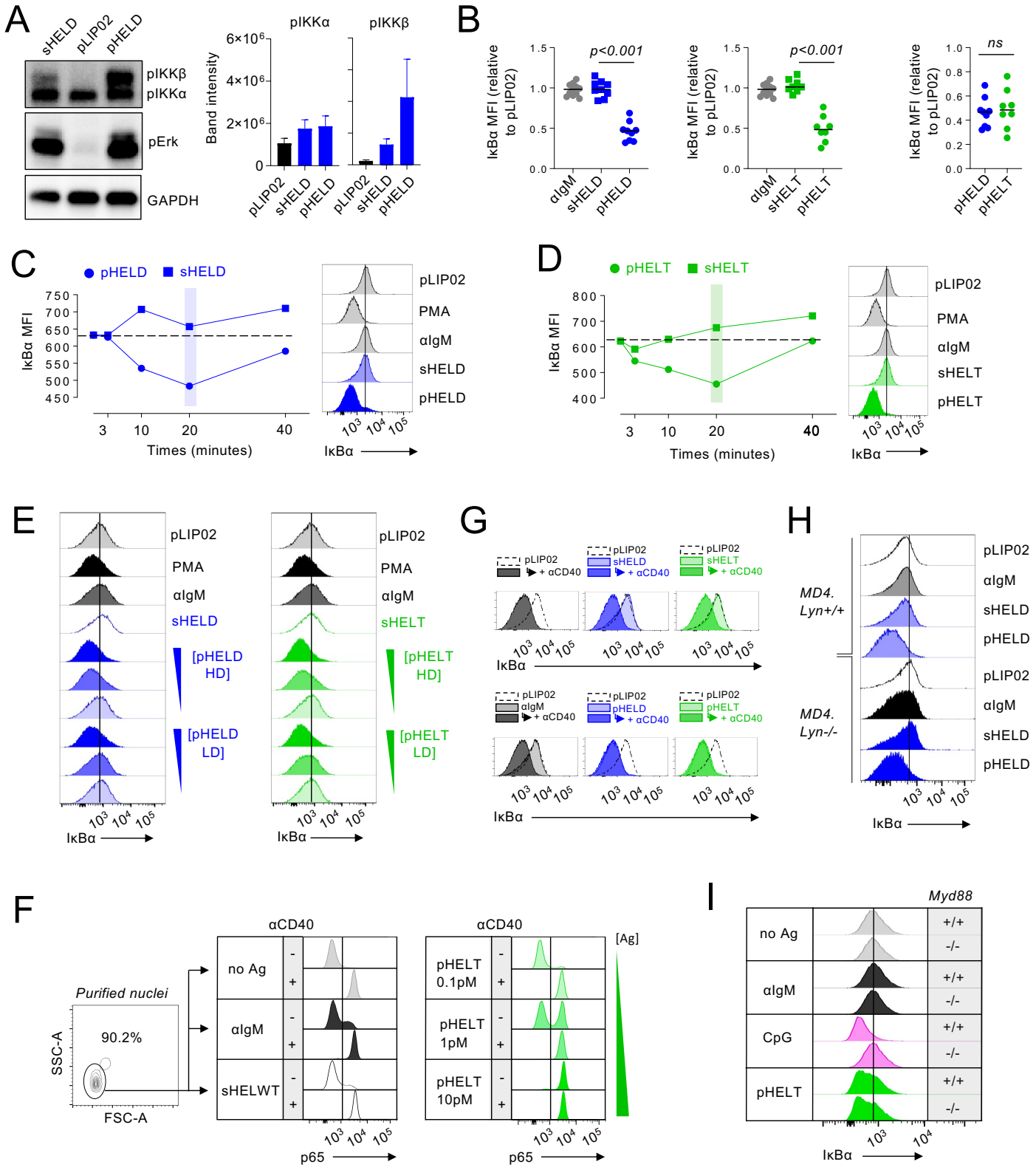

Figure 8. pHEL trigger robust proliferation with a lower NUR77-eGFP threshold than soluble stimuli

A. Pooled splenocytes and lymphocytes from MD4 mice were incubated with indicated stimuli for 24 hours, stained to detect B220+ cells and analysed by flow cytometry. Graphs depicting dose-response curve for FSC-A MFI (A) are representative of at least 4 independent experiments. Summary data correspond to 24 hr stimulation and show FSC-A values for highest concentration of sHELD/T and pHELD/T-HD in each individual experiment (1 μg/ml and 1pM respectively) for N=5-6 experiments. Lines connect samples from the same experiment. Groups were compared by a parametric paired T-test. **B.** Pooled splenocytes and lymphocytes from MD4 mice were incubated with indicated stimuli for 24 hours (anti-IgM 10 μg/ml, sHEL-WT 1 μg/ml, and pHELT-HD 1pM), and stained to detect B220 and either intra-cellular MYC or surface CD69 and CD86 expression by flow cytometry. Graphs depict MFI data pooled from 6 independent experiments +SEM. Pre-specified groups were compared by a parametric unpaired T-test. **C.** Viable frequencies of MD4 lymph node B cells in culture at 72-hours post-stimulation with sHELD/T and pHELD/T in the presence of 20ng/ml BAFF assessed via live/dead stain applied to parent B220+ gate. Each datapoint is an independent sample from >= 4 independent experiments; lines connect samples from the same experiment. Groups were compared by a parametric paired T-test. **D.** As in 4A, but cells were cultured with IRAK1/4 inhibitor (1μM) and indicated stimuli (CpG 2.5 μM, pHELT-HD 1pM) for 3hrs and then stained to detect intracellular MYC expression. Histograms are representative of 2 independent experiments as well as an additional 2 experiments assessing MYC at 24hrs +/– MYD88. **E.** As in B, except either *Myd88*+/+ or *Myd88*–/– MD4 cells were cultured with either 2.5 μM CpG or 1pM pHELT-HD for 24hr. Histograms depict surface CD69 expression among live B220+ cells and are representative of 3 independent experiments. **F, G.** MD4 NUR77-eGFP reporter lymph node cells were labelled with CTV and cultured with indicated stimuli (1 μg/ml sHELD/T, 1pM pHELD/T) for 72 hours with 20ng/ml BAFF +/– 10ng/ml IL-4. Neighbouring histograms show division peaks, arrowheads denoting changes in division peak intensity between IL-4-treated and untreated samples. Representative plots depict CTV dilution (x-axis) relative to NUR77-GFP expression (y-axis) among live B220+ B cells assessed by flow cytometry. Shaded bars reference NUR77-GFP levels in dividing B cells stimulated with soluble Ag (sHELD/sHELT). (Right) Quantification of NUR77-GFP levels in the first division peak (cells that have undergone a single round of division). Data without

IL-4 are representative of 5-7 independent experiments. Data comparing +/– IL-4 are representative of at least 4 independent experiments. **H.** As in F, but stained to detect intra-cellular C-MYC. Plots are representative of at least 3 independent experiments. **I. J.** Quantification of NUR77-GFP levels (I) and C-MYC (J) in the first division peak of polyclonal NUR77-eGFP reporter B cells cultured with anti-IgM 6.4μg/ml +/– 10ng/ml IL-4 as in S4E, H. Graph shows three biological replicates compared by parametric t-test. Data depicted are representative of > 6 independent experiments.

Figure 8. pHEL trigger robust proliferation with a lower Nur77-eGFP threshold than soluble stimuli

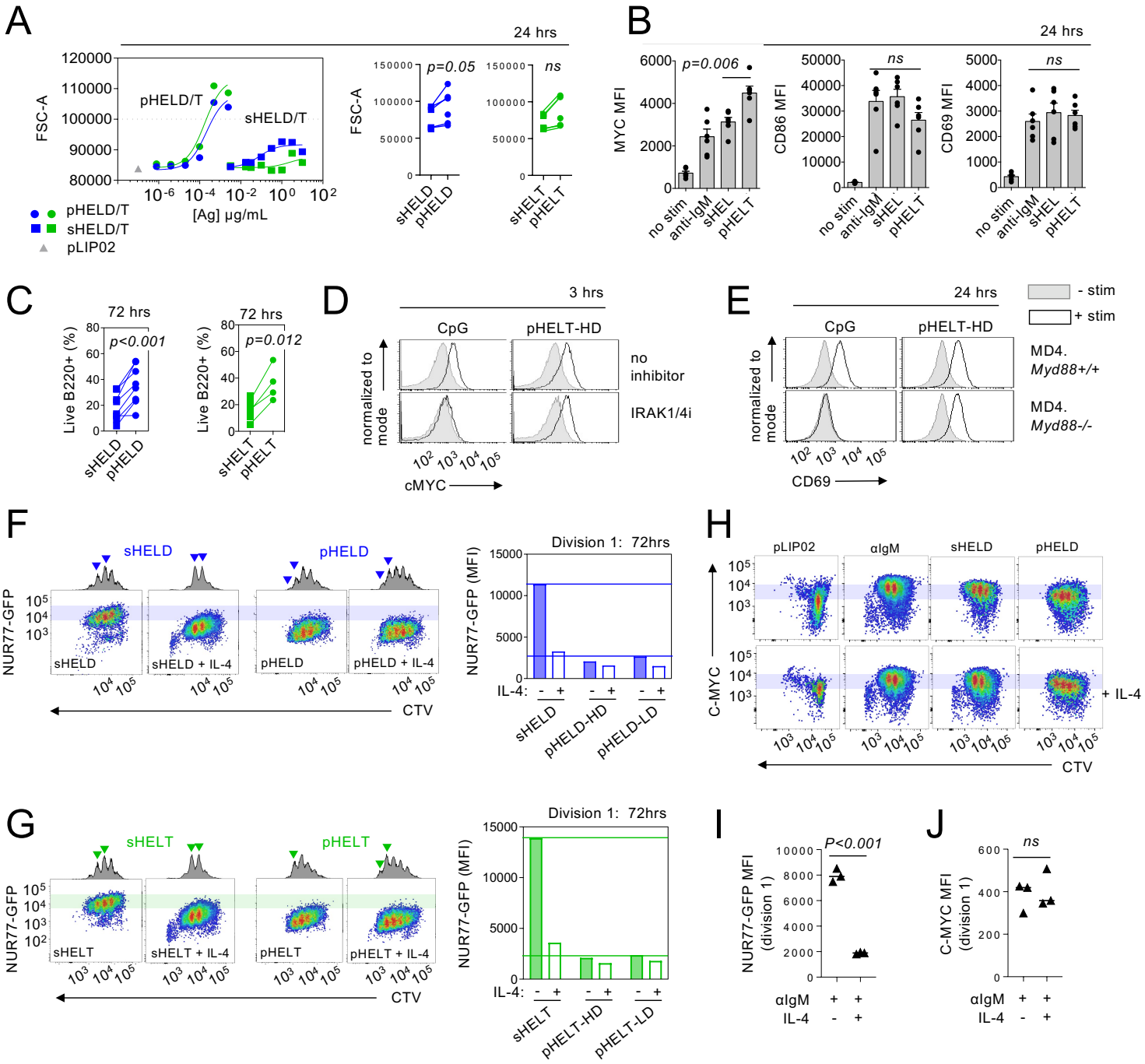

Supplementary Figure 1. Associated with Main Figure 1.

A. Hen egg lysozyme (HEL) was engineered with a c-terminal cysteine residue (yellow shadowing) that preserves native protein structure but allows stable conjugation in a fixed orientation to SVLS via maleimide chemistry. Point mutations (zoomed box) were also introduced into sHEL epitope which is bound by the Hy10 BCR and were previously described to reduce binding affinity[38]. HELD carrying two mutations or HELT carrying three mutations, along with the cysteine modification, were then purified from an overexpression system in E. coli. **B.** A library of SVLS was constructed with purified HELD or HELT conjugated at various densities to liposomes yielding pHELD/T particles with 3-500 antigenic epitopes per particle. Epitope density is calculated as [HEL]/[lip] in M. For pHELD/T with high ED 250-290, 1pM pHEL = 250-290nM HEL (~4ng/ml; 15.6kD HEL mol weight). **C.** Congenically-marked MD4 (Hy10) and wild-type splenocytes were stimulated with pHELD or a naked control particle (pLIP02). NUR77-GFP reporter expression along with congenic markers CD45.1/2 was analysed in B220+ cells 24 hours later as in Main Fig 1C. Axes were intentionally off-set to visualize lack of response to pLIP02/in wild-type B cells. **D.** NUR77-GFP reporter expression was analysed in MD4 B cells at 24 hours post-stimulation with the same batch of pHELD at various dates after its synthesis. Reporter expression was normalized to the pLIP02 condition in each experiment. **E.** As in main Fig 1E but with pHELT instead of pHELD at varying epitope densities. Data is from a single experiment and representative of at least 3 independent experiments. **F.** As in E, but stimulated with SVLS carrying high or ultra-low density of HELD or HELT. Data is from a single experiment. **G.** As in E, but CD69 was analysed at 24 hours post-stimulation with pHELD (left) or pHELT (right). Data are from a single experiment and representative of at least 3 independent experiments. Curves were modelled with three-parameter nonlinear regression (C, E, F, G).

Supplementary Figure 1. Extended data related to main Figure 1

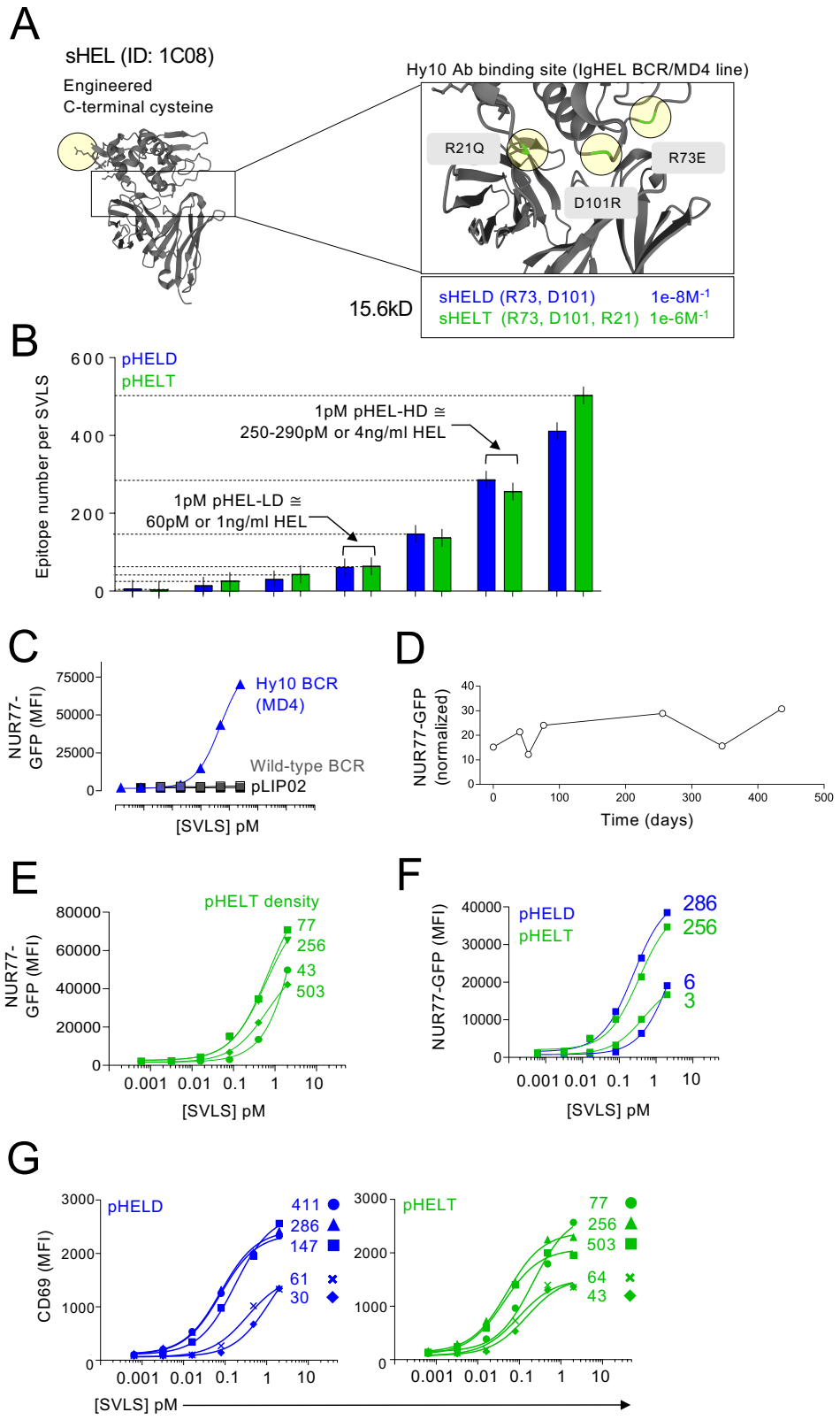

Supplementary Figure 2. Associated with Main Figure 2.

A, B. Pooled splenocytes and lymphocytes from MD4 mice were stimulated and stained as in Main Figure 2A, B but assessed for intra-cellular pS6 over a time course. Graphs (left) and histograms (middle) depict pS6 in B220+ cells from a single time course and is representative of at least 2 independent experiments. Graphs (right) depict B cell pS6 MFI after 20 min stimulation; each point represents an independent experiment and data are pooled >= 5 experiments depending on stimulus. **C.** Graph depicts pHELT and pHELD data from A, B graphed together for comparison. Pre-specified groups in A-C were compared by a paired parametric T-test. **D.** As in 2A, B but comparing pErk in stimulated B220+ splenocytes and lymph node cells separately at 20 mins. Histograms are from at least 2 independent experiments. **E-G**. As in 2A, but splenocytes were stained with B220, CD21, and CD23 and gated to identify pErk expression in B220+ subsets (E): immature T1 (CD21negCD23neg), marginal zone (CD21hiCD23int) and T2/T3/Follicular mature (CD23+CD21int). Representative histograms show pErk in gated subsets following sHEL-WT 1 μg/ml, 1pM pHELT-HD (ED 256), or PMA stimulation (F). Quantification of %pErk+ cells from three independent experiments (G). Groups were compared by one-way ANOVA. Data in E-G are representative of at least 8 independent experiments. **H, I.** Pooled MD4 splenocytes and lymphocytes were loaded with Indo-1 calcium indicator dye, stained with surface markers to detect B220+ subsets (H) as in S2E, and stimulated with anti-IgM (10 μg/ml), sHELD (1 μg/ml), or pHELD-HD (1pM). Calcium entry was assessed by flow cytometry for at least 3 minutes. Ratio of bound/unbound Indo-1 fluorescence over time is plotted (I). Data are representative of at least 4 independent experiments. **J.** As in Main Figure 3A, B except CD23+ B cells stimulated with pHELT-HD ED 256 and pHELT ultra low ED 3 are compared at 10, 1, 0.1pM doses. Data are representative of 4 independent experiments.

Supplementary Figure 2. Extended data related to main Figure 2

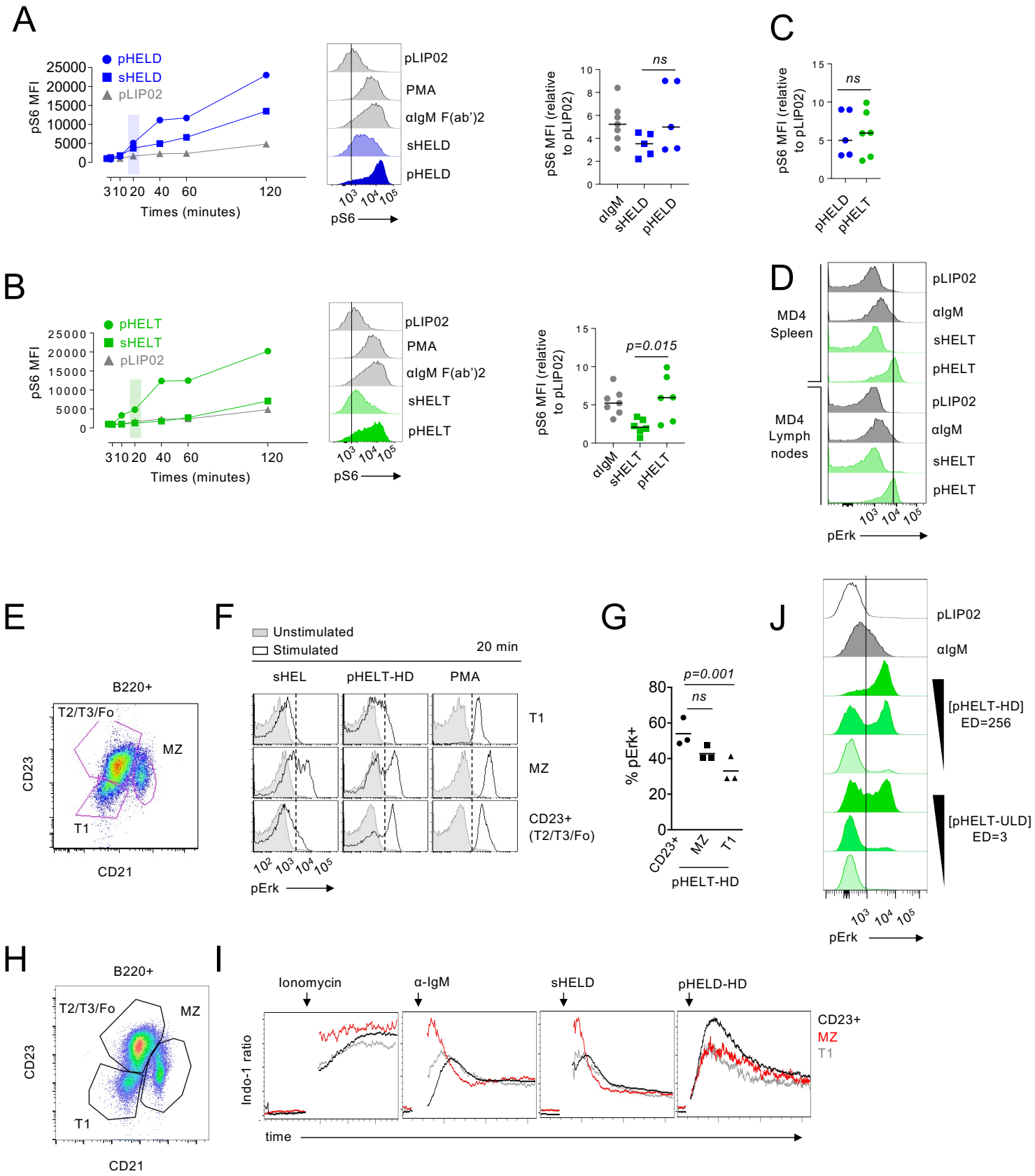

Supplementary Figure 3. Associated with Main Figure 6

A. As in Main Figure 6B, but with sHELT and pHELT (HD/LD 256, 64) stimuli. Data are representative of 4 independent experiments. **B.** As in Main Figure 6B, C, except pHELD ultra low ED 6 and pHELT ultra low ED 3 are used at 10pM and 1pM doses. Graph depicts data from 3 independent experiments. Pre-specified groups were compared by parametric T-tests and are plotted together on the same graph for convenience. **C.** As in Main Figure 6E, but with inclusion of anti-IgM 10 μg/ml as second stimulus following pHELD. Data are representative of 4 independent experiments. **D.** As in Main Figures 6F, G but with sHEL 1 μg/ml added in at peak calcium response following pHEL stimulation. Data are representative of at least 3 independent experiments. **E.** As in Main Figure 7I, but with LPS 10μg/ml, CpG 2.5μM, or anti-CD40 1μg/ml stimulation. Data are representative of 3 independent experiments.

Supplementary Figure 3. Extended data relating to main figure 6

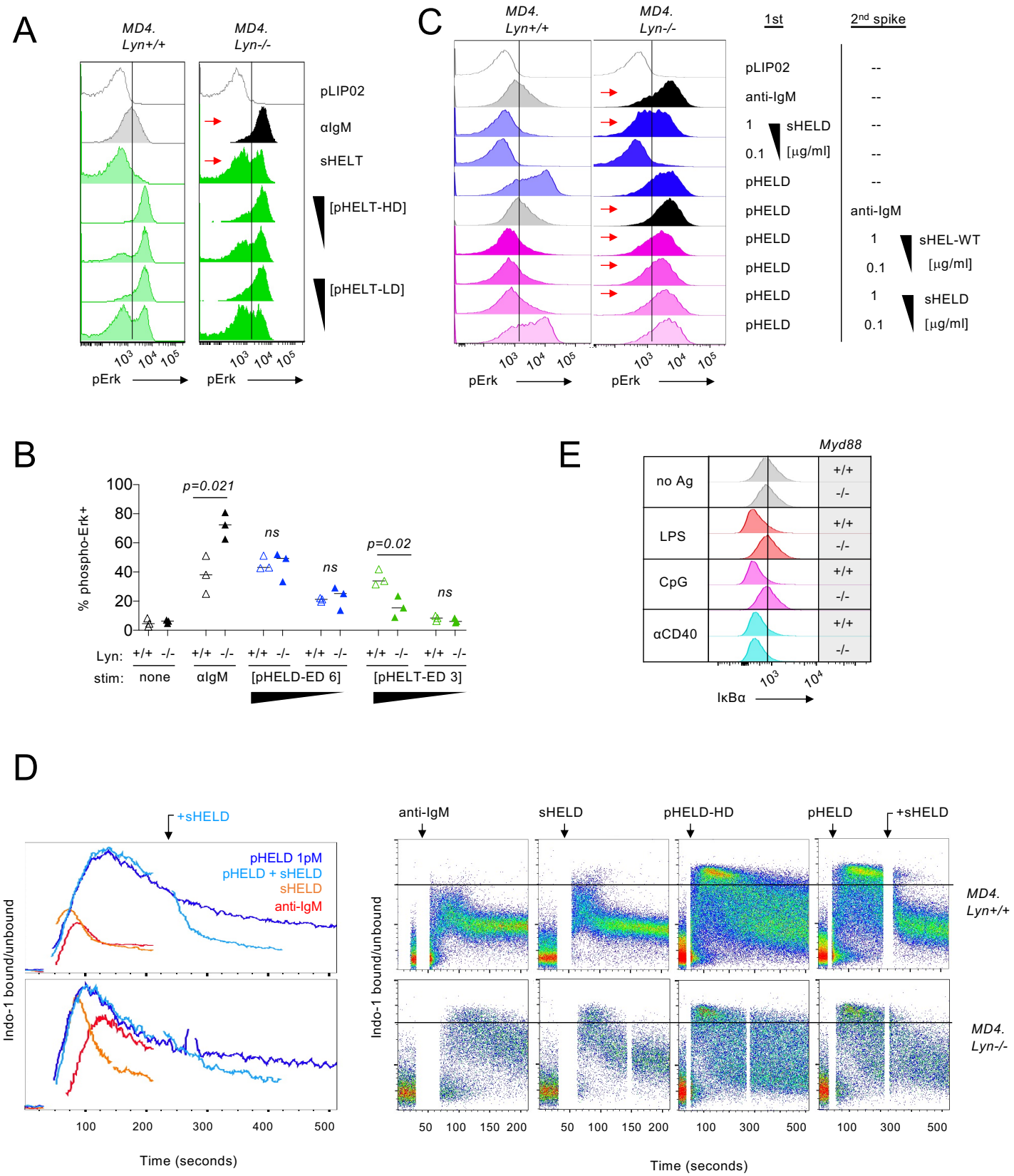

Supplementary Figure 4. Associated with Main Figure 8

A. Pooled splenocytes and lymphocytes from MD4 NUR77-eGFP reporter mice were cultured for 24 hr with sHELD 1μg/ml or pHELD-HD, LD (1pM), fixed, permeabilized, stained and analysed for GFP and intra-cellular C-MYC. A ratio of NUR77 and C-MYC among B220+ cells was calculated. Data plotted is from a single experiment and is representative of at least 3 independent experiments. **B.** MD4 pooled splenocytes and lymphocytes were cultured for 24 hr with anti-IgM 10μg/ml, sHELT 1μg/ml or pHELT-HD 1pM (without supplemental BAFF). Viable frequencies of MD4 B cells were assessed via live/dead stain. Each datapoint is an independent biological replicate. Groups were compared by a parametric T-test. **C.** As in Main Fig 8E except histograms depict FSC-A among live B220+ cells as a measure of cell growth and are representative of 4 independent experiments. **D.** NUR77-eGFP reporter splenocytes (top) or MD4.NUR77-eGFP splenocytes (middle and bottom) were loaded with vital dye CTV and cultured for 72 hours in the presence of either 6.4μg /ml anti-IgM or 30ng/ml sHEL (bottom), supplemented with 20ng/ml BAFF, and various concentrations of ibrutinib (0-50nM), and stained to detect viability and B220. Plots depict CTV and GFP expression in live B220+ B cells. Data are representative of at least 3 independent experiments. **E.** NUR77-eGFP reporter splenocytes cultured in the presence of 20ng/ml BAFF as in D except with varying doses of anti-IgM +/- 10ng/ml IL-4. Plots depict CTV and GFP expression in B220+ B cells. Data are representative of at least 6 independent experiments. **F.** As in Main Fig 8F, G MD4 NUR77-eGFP lymphocytes were cultures with stimuli + 20ng/ml BAFF for 72 hrs: 1 μg/ml sHELD/T, 1pM pHELD/T-HD or -LD. These data correspond to those depicted in Fig 8F, G but now include plots and quantification for pHELD/T-LD for direct comparison. Representative plots depict CTV dilution (x-axis) relative to NUR77-GFP expression (y-axis) among live B220+ B cells assessed by flow cytometry. Shaded bars reference NUR77-GFP levels in dividing B cells stimulated with soluble antigen (sHELD/sHELT). (Bottom) Quantification of NUR77-GFP levels in the first division peak (cells that have undergone a single round of division). Data are representative of 5-7 independent experiments. **G.** As in Main Fig 8H, but comparing intra-cellular C-MYC expression among live CTV-loaded B220+ B cells after 72hr culture across a range of doses: pHELT (1, 0.1, 0.01pM) and sHELT (500, 50, 5 ng/ml). Inset values represent MFI of division 1 cells in each plot. Data are representative of 3 independent experiments. **H.** As in E, but cultured with fixed 6.4 μg/ml dose of anti-IgM and titration of ibrutinib, and comparing C-MYC among live CTV-loaded B220+ B cells after 72hr culture. Data are representative of at least 6 independent experiments.

Supplementary Figure 4. Extended data relating to main figure 8

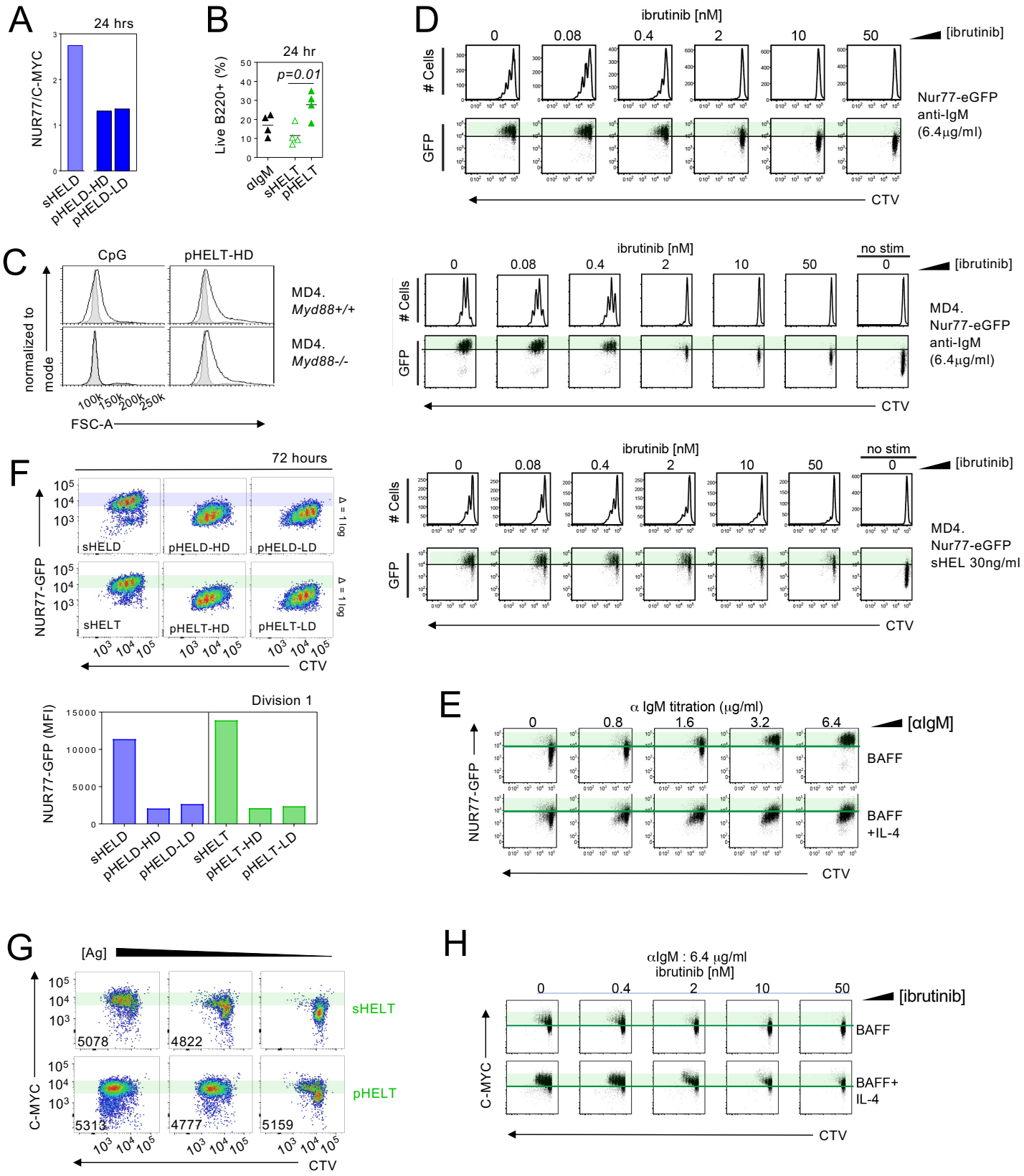

Supplementary Figure 5. Model.

A. Signalosome assembly in naïve B cells upon BCR stimulation by soluble Ag. BCR signal transduction requires sequential action of Src family kinases (SFKs) and SYK kinase. CD19 engagement amplifies PI3K activation. While multiple SFKs can mediate ITAM signaling downstream of the BCR, the SFK LYN plays a non-redundant role in phosphorylating ITIM-containing inhibitory coreceptors which in turn recruit PTPases SHP1 and SHIP1 that suppress PIP3. Dynamic regulation of PIP3 at the plasma membrane controls amplitude of signaling by recruiting downstream mediators including AKT, BTK, and PLCγ2 to orchestrate transcriptional programs mediated by NFAT, NF-κB and other factors.

B. SVLS with appropriately spaced epitopes robustly engage pre-existing BCR nanoclusters, but evade co-inhibitory receptors resulting in downstream signal amplification. SVLS do not rely upon CD19 engagement for signal amplification in vitro. In the absence of inhibitory PTPase engagement via ITIM -containing inhibitory receptors, PIP3 accumulates at the plasma membrane leading to enhanced and prolonged signalosome assembly and activity. Robust NFAT and NF-κB accumulation in the nucleus and AKT-dependent signals mimic co-stimulation and promote MYC expression, resulting in T-independent cell growth, survival and proliferation.
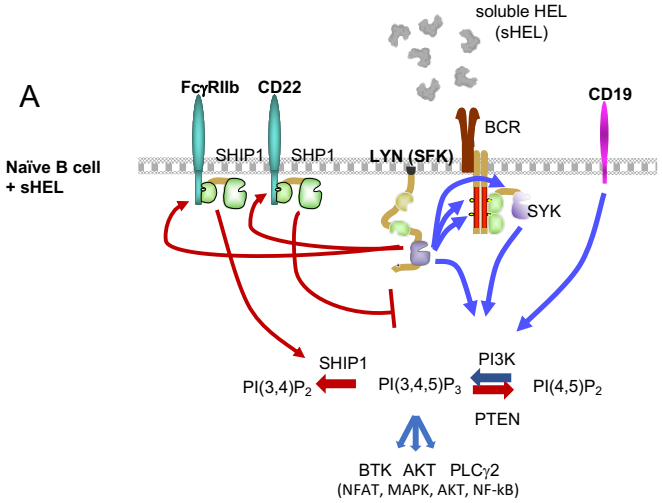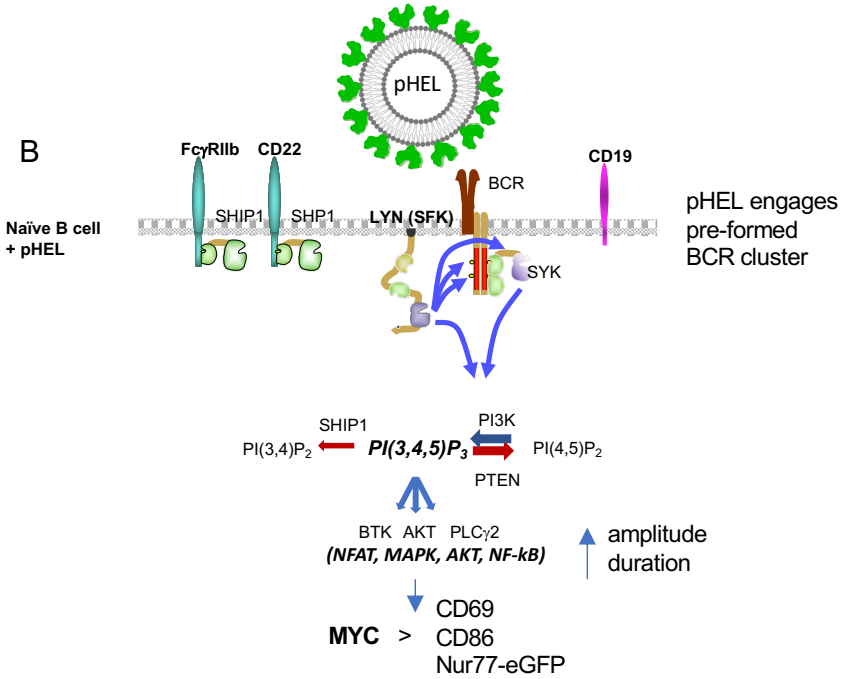
Supplementary Figure 5. Model